Physics of the Earth and Planetary Interiors 253 (2016) 5–20

Contents lists available at ScienceDirect

Physics of the Earth and Planetary Interiors

journal homepage: www.elsevier.com/locate/pepi

Paleomagnetism and dating of a thick lava pile in the Permian Bakaly formation of eastern Kazakhstan: Regularities and singularities of the paleomagnetic record in thick lava series

Mikhail L. Bazhenov[a,b,*], Rob Van der Voo[c], Zachary Menzo[c], Ada R. Dominguez[c], Joseph G. Meert[d], Natalia M. Levashova[a]

[a] Geological Institute, Russian Academy of Sciences, Moscow, Russia
[b] Institute of Physics of the Earth, Russian Academy of Sciences, Moscow, Russia
[c] Department of Earth and Environmental Sciences, University of Michigan, Ann Arbor, MI, USA
[d] Department of Geological Sciences, University of Florida, Gainesville, FL, USA

ARTICLE INFO

Article history:
Received 6 May 2015
Received in revised form 19 January 2016
Accepted 1 February 2016
Available online 15 February 2016

Keywords:
Paleomagnetism
Geochronology
Secular variation
Geomagnetic field
Asia
Permian

ABSTRACT

Paleomagnetic results on thick lava series are among the most important sources of information on the characteristics of ancient geomagnetic fields. Most paleo-secular variation data from lavas (PSVL) are of late Cenozoic age. There are far fewer results from lavas older than 5 Ma. The Central Asia Orogenic Belt that occupies several million square kilometers in Asia is probably the world's largest area of Paleozoic volcanism and is thus an attractive target for PSVL studies. We studied a ca. 1700 m thick lava pile in eastern Kazakhstan of Early Permian age. Magmatic zircons, successfully separated from an acid flow in this predominantly basaltic sequence, yielded an Early Permian age of 286.3 ± 3.5 Ma. Oriented samples were collected from 125 flows, resulting in 88 acceptable quality flow-means ($n \geqslant 4$ samples, radius of confidence circle $\alpha_{95} \leqslant 15°$) of the high-temperature magnetization component. The uniformly reversed component is pre-tilting and arguably of a primary origin. The overall mean direction has a declination = 242.0° and an inclination = −56.2° ($k = 71.5$, $\alpha_{95} = 1.8°$; $N = 88$ sites; pole at 44.1°N, 160.6°E, $A_{95} = 2.2°$). Our pole agrees well with the Early Permian reference data for Baltica, in accord with the radiometric age of the lava pile and geological views on evolution of the western part of the Central Asia Orogenic Belt. The new Early Permian result indicates a comparatively low level of secular variation especially when compared to PSVL data from intervals with frequent reversals. Still, the overall scatter of dispersion estimates that are used as proxies for SV magnitudes, elongation values and elongation orientations for PSVL data is high and cannot be fitted into any particular field model with fixed parameters. Both observed values and numerical simulations indicate that the main cause for the scatter of form parameters (elongation values and elongation orientations) is the too small size of collections. Dispersion estimates (concentration parameter and standard angular deviation) are more robust, and their scatter stems from other sources, which may include non-stochastic features of datasets like clusters, loops etc., or non-stationary behavior of secular variation magnitude over time intervals of many million years.

1. Introduction

It is a general belief that the most reliable information on past geomagnetic fields is derived from paleomagnetic studies of thick lava series and dike swarms. These datasets are referred to as "paleo-secular variation data from lavas", commonly abbreviated as PSVL. To date, most PSVL data are for the last 5 Ma, while far fewer studies are unevenly spread throughout the expanse of Earth history. Due to the limited temporal spread of PSVL studies, many intriguing hypotheses and assumptions regarding long-term evolutionary trends of the geomagnetic field are contentious.

Acquiring just one PSVL datum entails sampling of up to, or more than, a hundred sites, conducting detailed laboratory demagnetizations of hundreds of samples, and performing multi-stage analyses of the paleomagnetic data. In addition to being labor-intensive, it can be problematic to find field exposures that can

* Corresponding author at: Geological Institute, Russian Academy of Sciences, Moscow, Russia.
E-mail addresses: mibazh@mail.ru (M.L. Bazhenov), voo@umich.edu (R. Van der Voo), zmenzo@umich.edu (Z. Menzo), ardomin@umich.edu (A.R. Dominguez), jmeert@ufl.edu (J.G. Meert), namile2007@rambler.ru (N.M. Levashova).

http://dx.doi.org/10.1016/j.pepi.2016.02.001
0031-9201/

provide enough samples to conduct PSVL studies in deep time (i.e. pre-Cenozoic). Given these requirements, it is often the case that a paleomagnetic study with other aims in mind serves as an invaluable reconnaissance for a subsequent PSVL study.

The lower half of the studied section was sampled (one sample per flow) by Levashova et al. (2003) in order to find normal polarity intervals in the presumably Late Permian lava series (Sal'menova and Koshkin, 1990) of East Kazakhstan (Figs. 1 and 2). The results of the previous paleomagnetic study can be summarized as follows: (1) A single characteristic component, ChRM, was isolated from more than 90% of samples; (2) The ChRM is of reversed polarity and rather tightly grouped, no anomalous directions having been found; (3) The ChRM predates folding as indicated by the data from different fold limbs of the Bakanas Basin (A and B in Fig. 1a). (4) The paleomagnetic pole for section B was found to agree with the apparent polar wander path for Baltica, whereas the more deformed locality A was rotated some 20–30° clockwise. Thus, available paleomagnetic and geological data make this locality a promising object for a new PSVL study.

This paper presents an important new PSVL dataset for the undersampled Paleozoic Era. Bazhenov et al. (2014) published a partial dataset from these lavas and noted a very low level of angular dispersion in these data. In this paper, we report a comprehensive study of the entire sampled section along with an investigation of pre-Late Cenozoic PSVL studies in an effort to identify any emerging patterns.

2. Geological setting and sampling

Volcanic rocks with ages ranging from the Cambrian to the Permian are widespread in the Central Asian orogenic belt that covers much of middle Eurasia (Fig. 1a). In the western part of this belt (Kazakhstan), volcanic rocks accumulated in a variety of tectonic settings predominately subduction. Final ocean closure in the studied region took place in the Early Permian, although several isolated basins filled with subaerially erupted volcanics are located in East Kazakhstan (Fig. 1b; Khain, 1977; Levashova et al., 2012). Volcanism within these isolated areas is related to extension and subsidence following cessation of subduction (Peive and Mossakovskii, 1982; Tevelev, 2003). The lavas range in composition from basalt to rhyolite, mostly of subalkalic composition, and unconformably reside on older structures. Age constraints on these volcanics is almost entirely based on scarce fossil plants and pollen data and subsequent correlation of widely separated lava sections rather than isotopic ages (Lyapichev et al., 1993).

The Bakanas basin in eastern Kazakhstan is a typical example of a superposed basin (Fig. 1b). Here, Upper Carboniferous–Early Permian felsic volcanics and volcano-sedimentary units are overlain by the Bakaly Formation that forms the focus of our study (Fig. 2a). The Bakaly Formation (also known as the Bakalin Formation; Levashova et al., 2003) varies in thickness between 600 and 2600 m and predominantly consists of basalt and basaltic andesite with several thick sheets of acid lava and rare thin lenses of

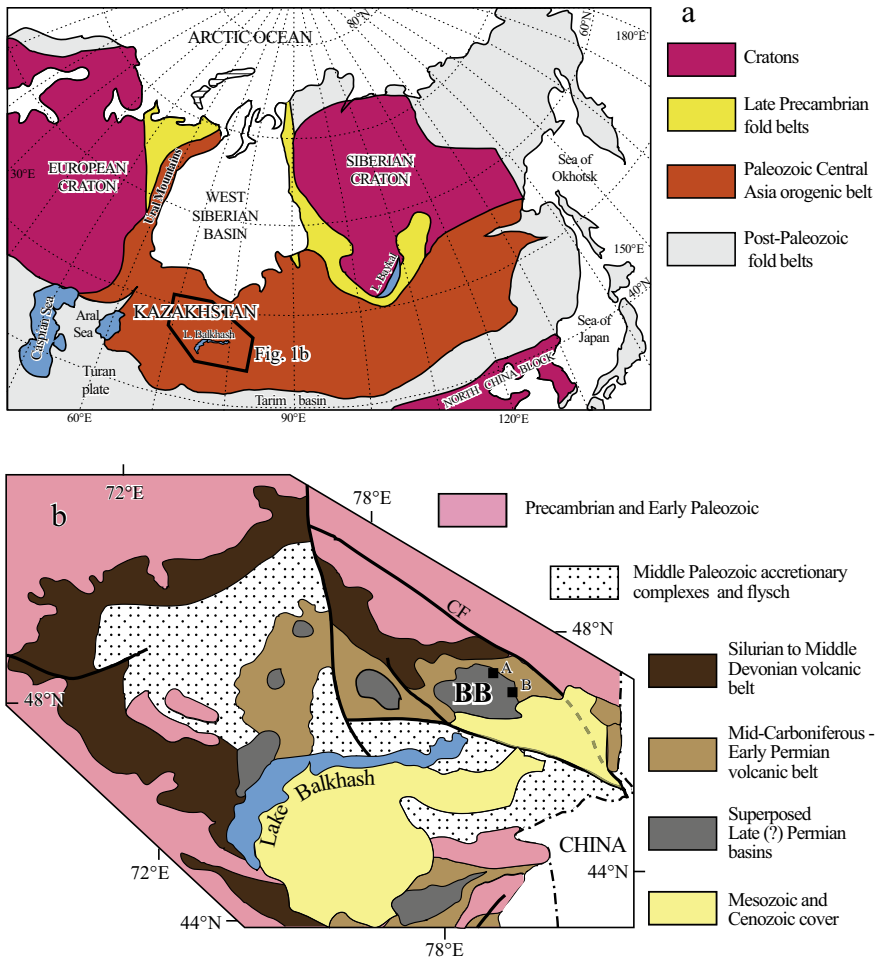

Fig. 1. (a) Major tectonic units of Northern Eurasia. (b) Schematic tectonic map of central-east Kazakhstan. Thick solid lines denote major faults (CF, Chingiz Fault). BB is the Bakanas Basin. Black squares A and B denote sampling localities from Levashova et al. (2003). (For interpretation of the references to color in this figure legend, the reader is referred to the web version of this article.)

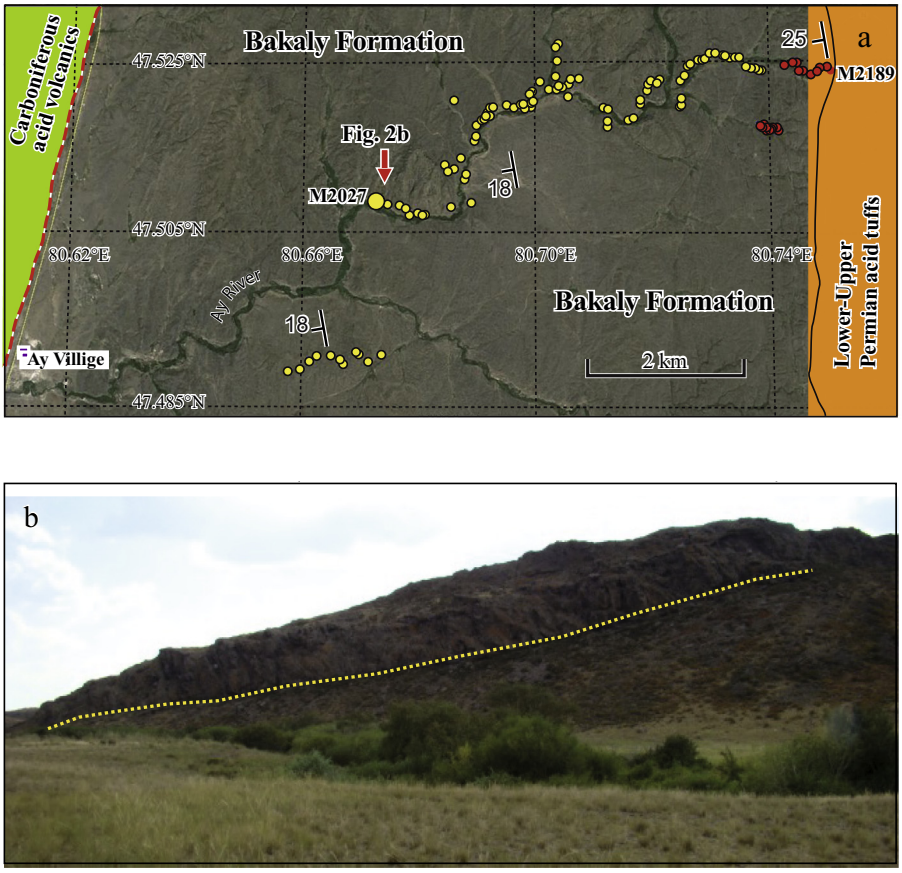

Fig. 2. (a) Geological map of the studied section of the Bakaly Fm. (square B in Fig. 1b). Yellow (red) circles denote sampling sites with average dip of 18° (steeper dip of 25°). (b) Conformable contact (yellow dotted line) between the series of thin basalt flows below and a thick trachy-rhyolite flow above (view to NW). (For interpretation of the references to color in this figure legend, the reader is referred to the web version of this article.)

coarse-grained sediments. The Bakaly volcanics are gently tilted at 10 to 25°; steeper dips and folds in some parts of the Bakanas basin are usually fault-conjugated. This deformation may either be related to movements along large strike-slip faults in the Late Triassic – Early Jurassic (Samygin, 1974) or coincide with a late regional tectonism in the Late Permian – Early Triassic.

The more than 2000 m thick section of the eastern flank of the Bakanas basin comprises several hundred 2–10 m thick flows of basalt and andesite-basalt (Fig. 2a), with few dacite flows, two of which are several tens of meters thick (Fig. 2b). Rare thin lenses of stratified coarse-grained sandstone and the most distinct flow boundaries were used to determine bedding attitudes. Mean dip-azimuth/dip-angle are 254°/18° (± 4°) for the main part of the section, while the dips are a bit steeper (254°/25°) at the section base (yellow and red circles in Fig. 2a, respectively). Additional structural control was derived from the strike of cuestas formed by the most resistant flows. Note also that basalt flows, which prevail through the section, rarely have noticeable primary tilts; so it is improbable for more acid lava to have them too. The Bakaly Fm. is conformably underlain by acid tuffs of presumed Early–Late Permian age (Sal'menova and Koshkin, 1990). In the west, the Bakaly Fm. is bounded by a fault (red dashed line in Fig. 2a), beyond which poorly stratified Carboniferous lavas are exposed.

The Tatarian age of the Bakaly Fm. was inferred on the basis of fossils (Sal'menova and Koshkin, 1990), but Levashova et al. (2003) expressed some reservations, speculating that the age was more likely Early Permian. Levashova et al. (2003) observed no normal-polarity directions in the lower half of the section (sites B1–B8; 9–12 flows per site; one sample per flow), and concluded that the section's well-defined characteristic remanence is not younger than the Kiaman or Permo-Carboniferous Reversed Superchron (PCRS).

The positive paleomagnetic results (Levashova et al., 2003) combined with the thickness of the section prompted us to carry out a new paleomagnetic study of this lava series. A long sampling traverse was jointly carried out in August, 2011 by the Moscow paleomagnetists ("M" sites) and the Michigan team ("A" sites). Combined, these collections included 123 basalt and two acid flows (a flow = a site) from the base of the Bakaly Fm. through a total of 1600–1700 m (Fig. 2a). Each second or third flow was sampled, although some longer intervals were likely missed due to outcrop distribution. Thus, the conservative estimate is that the total number of flows is >300. Although described by Sal'menova and Koshkin (1990), no interbedded conglomerates were encountered for a paleomagnetic conglomerate test.

Initially, our intention was to take 7–8 samples per site, either as hand blocks (M-sites) to be subsequently cut into 2 cm cubes or as drilled cores (A-sites). Due to an equipment failure (drill), most A-sites were collected as oriented hand samples (four samples per site) and were returned to Ann Arbor where cylindrical specimens were drilled. Most samples were oriented with a magnetic compass; no examples of outcrops affecting compass readings were observed. GPS-recorded site locations, field observations, and structural data were used to arrange the sites in stratigraphic order (Fig. 2a; Table A1 in Supplements).

3. Geochronology

3.1. Methods

Two samples of acid volcanic rocks were collected from within the sequence. A relatively thin acid tuff from the base of the section yielded only a few rounded and broken zircons that were not analyzed. Sample M2027 was taken from a thicker acid flow in the middle of the section. A total of ~50 zircons/zircon pieces ranging in size from 10 μm to 240 μm were separated using mechanical and density methods and then hand-picked. Zircons were then mounted into an epoxy plug and polished to expose their surfaces. The epoxy plugs were sonicated and cleaned in nitric acid to remove any common Pb surface contamination. Cathodoluminescence (CL) images were then taken using an SEM (Scanning Electron Microscope) in addition to reflected light microscopic images. The zircons were generally clear, euhedral to subhedral grains that exhibit some zoning seen in the CL imagery (Fig. 3a–c).

Zircon U–Pb isotopic analyses were conducted at the Department of Geological Sciences (University of Florida) on a Nu Plasma multi-collector plasma source mass spectrometer equipped with three ion counters and 12 Faraday detectors. The LA–ICPMC–MS is equipped with a specially designed collector block for simultaneous acquisition of ^{204}Pb (^{204}Hg), ^{206}Pb and ^{207}Pb signals on the ion-counting detectors and ^{235}U and ^{238}U on the Faraday detectors (Mueller et al., 2008). Mounted zircon grains were laser ablated using a New-Wave 213 nm ultraviolet laser beam. During U–Pb analyses, the sample was decrepitated in a He stream and then mixed with Ar-gas for induction into the mass spectrometer. Background measurements were performed before each analysis for blank correction and contributions from ^{204}Hg. Each sample was ablated for ~30 s in an effort to minimize pit depth and fractionation. Data calibration and drift corrections were conducted using the FC-1 Duluth Gabbro zircon standard, and long-term reproducibility was 2% for ^{206}Pb/^{238}U (2σ) and 1% for ^{207}Pb/^{206}Pb (2σ) ages (Mueller et al., 2008). Common Pb was monitored by comparing the ^{204}Pb count in the standard to those of the samples. Samples with significantly higher (>25%) ^{204}Pb counts were not used in the analysis. Data reduction and correction were conducted using a combination of in-house software and Isoplot (Ludwig, 2008).

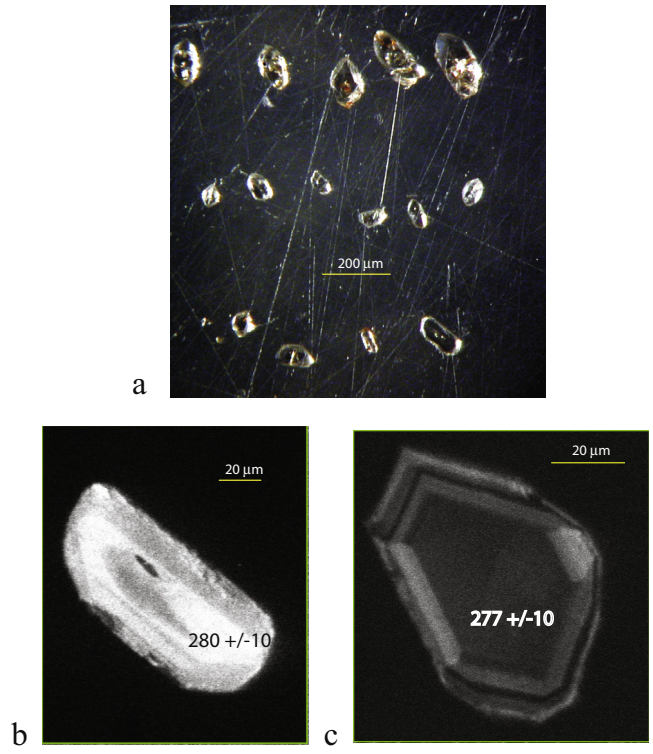

Fig. 3. (a) Reflected light image of several zircon/zircon pieces from sample M2027. (b) CL image of zircon 2027-17b that yielded a ^{238}U/^{206}Pb age of 280 ± 10 Ma (brighter core portion of the crystal) and (c) zoned zircon 2027-13b that yielded a ^{238}U/^{206}Pb age of 277 ± 10 Ma (darker center portion of the crystal).

3.2. Results

Of the approximately 50 zircons that were separated, interpretable results were obtained from 22 different grains (Table 1). Other zircons were too small to analyze with our laser (i.e. those <30 μm in size), had discordance between the ^{206}Pb/^{238}U and ^{207}Pb/^{235}U ages of greater than 10 percent, or showed high ^{204}Pb counts compared to the standards. Fig. 4a shows the analyses in a Tera–Wasserburg plot with a lower intercept of 281.3 ± 8.4 Ma (MSWD = 1.6) for 21/22 analyses (Table 1). The best estimate for the age of crystallization of the zircons is given by the weighted mean ^{238}U/^{206}Pb age (Fig. 4b) at 286.3 ± 3.5 Ma, which corresponds to mid-Early Permian time (Artinskian stage). The above age is statistically identical to the preliminary age of 283.0 ± 2.4 Ma reported by Bazhenov et al. (2014).

4. Paleomagnetic study

4.1. Methods

Cubic specimens from the "M" sites were measured using JR-4 and JR-6 spinner magnetometers at the Geological Institute of the Russian Academy of Science in Moscow. The spinner magnetometers have a noise level of 0.05 mAm^{-1}. The magnetometers are housed inside large Helmholtz coils to reduce the ambient magnetic field. One specimen from each hand-sample was stepwise demagnetized in homemade ovens with internal residual fields of approximately 10 nT. In the paleomagnetic laboratory of the University of Michigan, field- and laboratory-drilled cylindrical cores with 25 mm diameter were sliced into standard 20 mm high cylinders. The specimens were stepwise demagnetized utilizing an Analytical Services TD-48 thermal demagnetizer with internal residual fields of <10 nT, or in treatments up to 200 mT with a Sapphire Instruments SI-4 AF demagnetizer. Measurements were carried out with a 2G Enterprises cryogenic magnetometer in a magnetically shielded room with a rest field typically less than 200 nT. Thermal demagnetizations were carried out in both laboratories in 15–20 increments up to 700 °C. A-site characteristic magnetization data constituted the Honors thesis of Mr. Zachary Menzo (2013), which is on file at the University of Michigan website. No systematic difference was found between the sample magnetizations that were measured in Moscow or Ann Arbor, and the data have been pooled.

Demagnetization results were plotted on orthogonal vector diagrams (Zijderveld, 1967), and linear trajectories were used to determine directions of magnetic components by a least-squares fit comprising three or more measurements (Kirschvink, 1980). The characteristic remanent magnetization, ChRM, was determined with anchoring of the final linear segments to the origin of the vector diagrams in most samples. In less than 5% of the collection, convincing isolation of the ChRM was not reached, and joint analysis of remagnetization circles and component directions defined by linear trajectories decaying towards the origin were used to calculate site-means (McFadden and McElhinny, 1988). Paleomagnetic analyses and calculations were carried out with the PaleoMac software (Cogné, 2003). The software package

Table 1
U–Pb ICP–MS results.

Grain Name	$^{207}Pb/^{235}U$	2σ	$^{206}Pb/^{238}U$	2σ	(error corr.)	$^{207}Pb/^{206}Pb$	2σ	$^{206}Pb/^{238}U$ (Age) Ma	$^{*}2\sigma$	$^{207}Pb/^{235}U$ (Age) Ma	$^{*}2\sigma$	$^{207}Pb/^{206}Pb$ (Age) Ma	$^{*}2\sigma$	Discordance[1]
2027-3a[#]	0.39575	6	0.04914	6	0.95	0.05841	2	309	18	339	18	545	44	9
2027-5a	0.36776	6	0.04681	5	0.90	0.05698	2	295	15	318	15	491	54	7
2027-6a	0.36776	6	0.04681	5	0.90	0.05698	2	295	15	318	15	491	54	7
2027-7a	0.37573	5	0.04621	4	0.83	0.05897	3	291	12	324	14	566	63	10
2027-8a	0.38552	6	0.04816	5	0.84	0.05806	3	303	15	331	17	532	70	8
2027-10a	0.37433	5	0.04719	4	0.83	0.05753	3	297	11	323	13	512	57	8
2027_12a	0.34269	5	0.04446	4	0.84	0.05590	3	281	11	299	12	448	59	6
2027_14a	0.33998	5	0.04342	4	0.75	0.05679	3	274	10	297	13	483	71	8
2027_15a	0.33707	5	0.04460	5	0.92	0.05482	2	281	13	295	13	405	44	5
2027_16a	0.33915	6	0.04473	4	0.78	0.05499	4	282	12	296	15	412	80	5
2027_19a	0.33126	5	0.04481	5	0.91	0.05361	2	283	13	290	13	355	46	3
2027_20a	0.34456	5	0.04599	5	0.94	0.05434	2	290	14	301	14	385	41	3
2027_02b	0.36244	5	0.04700	5	0.91	0.05593	2	296	14	314	15	450	52	6
2027-3b	0.36952	5	0.04624	4	0.89	0.05796	2	292	13	319	14	528	50	9
2027_04b	0.36691	5	0.04527	4	0.81	0.05879	3	286	11	317	13	559	64	10
2027_06b	0.34638	6	0.04533	4	0.69	0.05542	5	286	12	302	17	429	104	5
2027_07b	0.35132	5	0.04631	4	0.91	0.05502	2	292	13	306	13	413	45	4
2027_09b	0.38411	8	0.04691	5	0.70	0.05939	5	296	15	330	21	581	118	10
2027_13b	0.34926	5	0.04395	4	0.77	0.05764	3	277	10	304	13	516	70	9
2027_16b	0.35189	5	0.04509	4	0.86	0.05661	3	285	12	306	14	476	59	7
2027_17b	0.36016	6	0.04434	4	0.63	0.05890	4	280	10	312	15	564	96	10
2027_20b	0.36323	5	0.04473	4	0.83	0.05889	3	282	11	315	13	563	58	10

2σ errors in $^{207}Pb/^{235}Pb$, $^{206}U/^{238}U$ and $^{207}Pb/^{206}Pb$ are given as percentages. $^{*}2\sigma$ errors on $^{206}Pb/^{238}U$, $^{207}Pb/^{235}U$ and $^{207}Pb/^{206}Pb$ ages are in Ma. Weighted mean $^{238}U/^{206}Pb$ weighted mean age = 286 ± 3.5 Ma (1 of 22 rejected, 95% confidence, MSWD = 1.6 probability = 0.05). [1]Discordance in percent between the calculated $^{206}Pb/^{238}U$ age and the $^{207}Pb/^{235}U$ age.
[#] rejected sample.

PmagPy by the MagIC Database Team was used for numerical simulations, particularly for computing predictions of the TK03.GAD model (Tauxe and Kent, 2004). To exclude anomalous data, the site-means were converted to VGPs and the most common 45° cutoff was applied to both simulated and observed data sets. In this paper, we calculated the elongation E, using the bivariate statistics (LeGoff, 1990) that produces two values of concentration parameter along main axes of inertia (there is a special option in PaleoMac software of Cogné, 2003). Our analysis shows that different ways of determining elongation values agree within 0.01–0.02.

4.2. Directional analysis

The intensity of natural remanent magnetization (NRM) ranges from 0.01 to >10 A/m in the volcanic rocks of the Bakaly Fm. and is the summation of two components in varying proportion (Fig. 5). A low-temperature component (LTC) is usually removed below 300–350 °C, but in some cases may persist up to 500 °C. LTC directions are reasonably grouped at many sites, and the overall mean direction ($D = 351°$, $I = 62.5°$, $\alpha_{95} = 5°$, $N = 54$ sites) is close to the present-day co-axial dipole field ($D = 0°$, $I = 62°$) in the area. This remanence is likely of recent viscous origin, perhaps with some contributions from "weathering" components.

Although the LTC can occasionally account for >90% of the NRM, a high-temperature ChRM is reliably isolated even in such samples, as shown in Fig. 5a. Typically, the LTC is much weaker, or absent altogether, and ChRM's are readily isolated in nearly all of these samples, with almost noiseless demagnetization trajectories (Fig. 5b–g). In several samples the remanence decay is noisier, but the ChRM can still be isolated unambiguously (Fig. 5h).

Without a single exception, the ChRM is of reversed polarity over the entire studied interval of >1600 m. At most sites, ChRM directions are well grouped, with concentration parameter (k) values ranging from 30 to >500, and averaging about 100. Judging by unblocking spectra, the ChRM may reside in nearly pure magnetite (Fig. 5b and c), nearly pure hematite (Fig. 5d and e), or both (Fig. 5f and g). Where both minerals are the ChRM carriers, the directions of the "magnetite" and "hematite" components are identical (Fig. 5f and g). Such a pattern is often attributed to high-temperature oxidation of magnetite during, or immediately after, lava emplacement (Levashova et al., 2009; Swanson-Hysell et al., 2009; Bazhenov et al., 2013). Rock-magnetic and paleointensity studies on the same section of the Bakaly Fm. (Shcherbakova et al., 2005) also provided evidence as to the primary origin of the remanence in these rocks.

Out of 125 sites sampled, 19 were rejected because their HTC was isolated in just one or two samples, or the directions are scattered (boldface entries in italics without directions and statistical parameters in Supplemental Table A1). Thus, means were computed for 106 sites (ALL in Table 2; Table A1 in Supplements). Of the remaining site means, 18 are either based on less than four samples or have $\alpha_{95} > 15°$, and were discarded (BAD in Table 2; Table A1) thus leaving us with 88 unit vectors of acceptable quality (GOOD-1 in Table 2). One more filtering step was taken for the sites with $k > 50$ (GOOD-2 in Table 2). Finally, only site-means with $\alpha_{95} < 10°$ are retained (BEST in Table 2). Upon conversion to poles, no VGPs were rejected with 45° cutoff at any stage of analysis.

The four result categories BEST, GOOD-1, GOOD-2 and BAD in Table 2 are statistically identical which means that the large scatter of the BAD category is mostly due to inadequate averaging of paleomagnetic noise in the poorly defined site-means. Although the k value for the BEST dataset is a little higher than for the GOOD ones, the difference is small. Hence we feel justified to use the GOOD-1 dataset in the subsequent analyses, as a reasonable balance between the overall statistics and the precision of each unit vector.

4.3. Angular dispersions, s, and concentration parameters, k

The residual within-site scatter may affect the k values in Table 2, a possible distortion by this dispersion may be evaluated with the aid of the following equation:

$$1/k_{\text{field}} = 1/k_{\text{total}} - 1/\bar{k}_{\text{site}}/\bar{n},$$

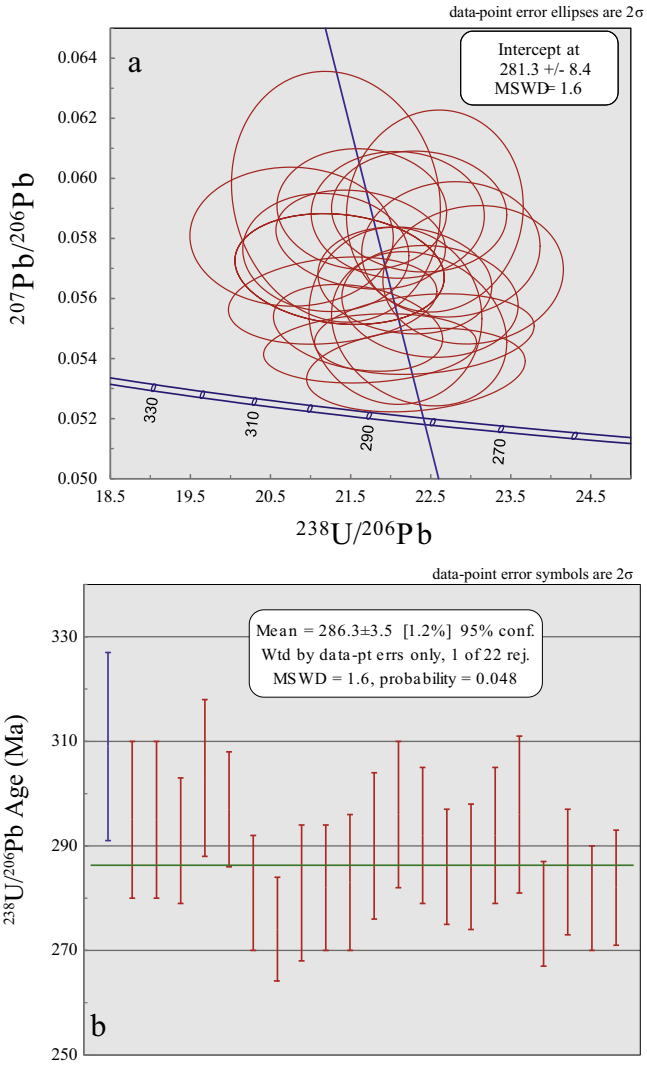

Fig. 4. (a) Tera–Wasserburg plot of 21 zircon laser spots with a lower intercept age of 281.3 ± 8.4 Ma and (b) Weighted mean plot of all 22 grains that yielded a $^{238}U/^{206}Pb$ mean age of 286.3 ± 3.5 Ma (MSWD = 1.6). Blue color represents a rejected analysis (zircon 2027-3a). (For interpretation of the references to color in this figure legend, the reader is referred to the web version of this article.).

where k_{field} is the SV-related scatter, k_{total} is the observed angular dispersion, k_{site} is within-site angular dispersion, and n is the number of samples. In this equation, the bar-*k* and bar-*n* parameters are the average values of the within-site concentration parameter and the number of samples in each lava flow. This formula gives k_{field} of 79.8 for the GOOD-1 dataset, which is statistically indistinguishable from k_{total}. Perhaps, the best estimate of the scatter of paleomagnetic directions is a cautiously conservative statement that k_{field} is close to 80.

4.4. Grouping

If not more than a few centuries have elapsed between emplacement of consecutive lava flows, the angular difference between their remanence directions will be statistically indiscernible (e.g., Riisager et al., 2003; Chenet et al., 2009). Hence, a common practice is to replace the stratigraphically ordered and tightly grouped site-means (directional group or DG) with a single group-mean that can be regarded as a spot-reading of the field. Following this practice, DG's were identified in the studied section using GOOD-1 data (Table A1). The resulting dataset of 16 DGs and 29 site-means (GOOD-1 & DG in Table 2) is somewhat more dispersed than the other result categories in this table.

Note, however, that the method of DG identification is efficient only for relatively diffuse datasets with *k* values of about 40 or less, simply because the confidence limits of the site-means are much less than the typical angular differences between the adjacent site-means. It is not so in our dataset (GOOD-1 in Table 2), where the average α_{95} of ~8° is comparable to the average angular distance between adjacent unit vectors of ~10° for the entire dataset. Hence it is quite likely that two adjacent flows may accidentally have statistically similar directions, those with larger confidence circles in particular. This random grouping is especially likely for directions in the most densely "populated" central part of the distribution (Fig. 6b), where the share of randomly created DG's may be rather high. Thus replacing the site-means with DG-means leads to preferential depopulation of tighter grouped data and general increase of dispersion.

There are some indications that random grouping does occur. First, we mostly sampled each second or third flow, with even longer gaps in some places (Fig. 2a). Additional gaps were created when the worst defined results were omitted. Despite, some formally recognized groups incorporate the sites spread over several ten meters or even more. Second, the volcanic outbursts could occur irrespectively of whether field direction was close to the average one or deviated from it. In our case, however, all DGs comprise the data from the central part of the distribution. According to our estimates, an acceptably sure separation of true and false DGs would have been probable if most site-means had had $\alpha_{95} < 5°$. In our case, it means ten or more samples per site, which is much more than what we have. Because of this issue, we disregard DG's in this paper, and the result based on site-means (GOOD-1 in Table 2) is used for further analysis.

4.5. Age of magnetization

The observed slight increase in data grouping upon tilt correction does not constitute a positive tilt test (Table 2; Fig. 6a and b); however, Levashova et al. (2003) reported paleomagnetic results on the same formation from two localities within the Bakanas Basin (Fig. 1b) and were able to establish the pre-folding age of the ChRM in the Bakaly volcanics.

The GOOD-1 mean direction is compared with reference directions recalculated to the study area from the 140 to 310 Ma segment of the apparent polar wander path (APWP) for Baltica (Torsvik et al., 2012). Our observed mean direction falls very close to the APWP and best agrees with the 280 Ma reference direction, deviating from it by 3.8° ± 2.5° (Fig. 6c). Although this deviation is statistically significant at the 95% level, the difference may stem from a variety of causes. It is worth noting that the APWP for Baltica is based entirely on paleomagnetic data from localities that are several thousand km away from the study area, and the tight match of the APWP and the Bakaly pole points to a very high degree of dipolarity of the Early Permian geomagnetic field, as was earlier already demonstrated for Late Permian time (Bazhenov et al., 2008). Note also that the GOOD-1 result differs from steeper and more southerly younger reference data (Fig. 6c). This similarity in the 280 Ma paleomagnetic poles from our study and Baltica is also consistent with the new radiometric age of the Bakaly Fm reported in this paper.

Thus we conclude that the ChRM in the Bakaly Fm. is prefolding. Its ubiquitously reversed polarity agrees with its acquisition at about 280 Myr during the PCRS, and its mean direction is very close to the nearly coeval reference direction for Baltica. These lines of evidence strongly indicate the primary origin of the ChRM in the studied volcanics.

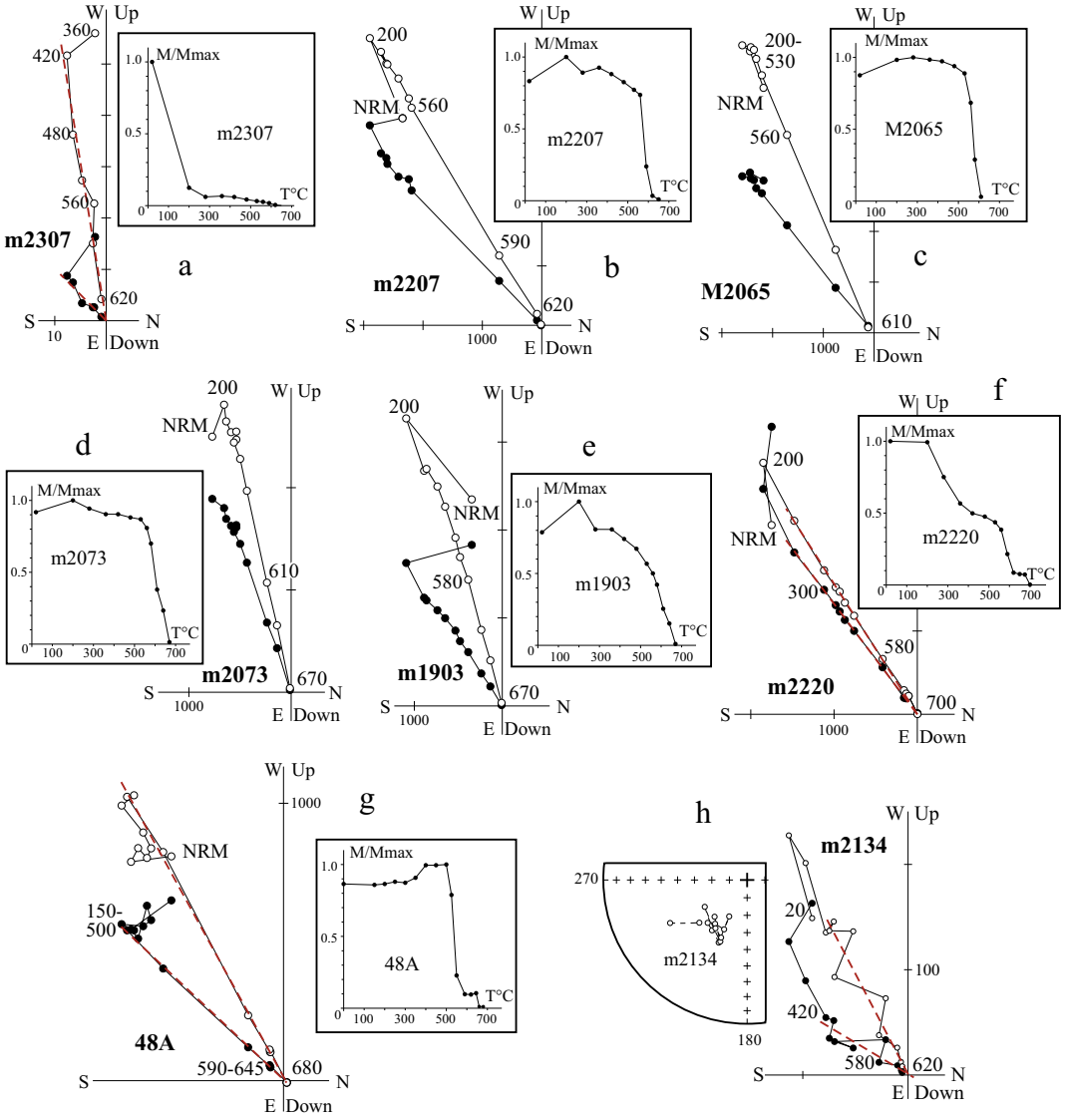

Fig. 5. Representative thermal demagnetization plots of the Permian volcanic rocks after tilt correction. Red dashed lines highlight the ChRMs on some plots for clarity. Full (open) dots represent vector endpoints projected onto the horizontal (vertical) plane. Temperature steps are in degrees Celsius. Magnetization intensities are in mA/m. For clarity, NRM points are omitted from some plots. Also shown are the plots of normalized NRM intensity (a–g) or stereoplot of vector end-points (h). (For interpretation of the references to color in this figure legend, the reader is referred to the web version of this article.)

5. SV averaging

The crucial question for a PSVL study is how well secular variation, SV, is averaged. This task is relatively easy for thick sedimentary sections, especially if substantiated by stratigraphic data, but is a tricky business for purely volcanic sections with magnetizations of the same polarity. As noted above, the total number of cooling units most likely exceeds 300. The large number of accepted site-means spread over the ~1600 m thick section does point to a rather long time interval covered by sampling. The agreement between the observed and reference directions also suggests that the averaging of SV within the collection is adequate. Neither observation, however, explicitly proves it.

Recently, Biggin et al. (2008a) suggested testing whether angular differences (Δ°) between adjacent site-means are serially correlated defining a non-random-ordering factor or 'NRO-factor'. For our collection, the NRO factor is significant at the level of >99%, thus indicating a significant degree of non-randomness, although the plot of Δ° does not show obvious "regularities" (Fig. 7a). So, we agree with Biggin et al. (2008a) that "while a lack of serial correlation in a large dataset implies that PSV must be well represented, the converse is not true: the presence of serial correlation, particularly in a large dataset, does not make an under-representation of the time-averaged field indubitable". For instance, if many consecutive directions form loops or tight clusters, the correlation will be significant but SV is adequately averaged in the entire dataset.

Jarboe et al. (2008) searched for "excessive regularities" like loops or long swathes in their PSVL dataset from the Steens Mountain (Oregon, USA) under an assumption that such features are created during quick successive emplacement of lava flows. We plotted a trajectory for the GOOD dataset of 88 stratigraphically ordered site-means; for better visibility, it is divided into eight differently colored segments (Fig. 7b). The as different segments do not overlap, e.g., black (## 1–11) and purple (## 77–88), or red (## 33–44)and yellow (## 44–55) thus indicating that the pattern is not perfectly random. At the same time, no loops or regular swathes of more than three consecutive points are found in the record which, on the whole, looks random.

Table 2
Mean paleomagnetic directions in lavas of the Bakaly Formation.

Name	N	In Situ				Tilt-corrected			
		D°	I°	k	α_{95}°	D°	I°	k	α_{95}°
ALL	106	248.1	−36.9	47.9	2.0	245.7	−55.9	54.7	1.9
BAD	18	253.3	−35.3	26.8	6.8	253.1	−53.7	26.8	6.8
GOOD-1	88	245.5	−37.1	57.7	2.0	242.0	−56.2	71.5	1.8
GOOD-1&DG	47	246.3	−36.4	48.9	3.0	243.2	−55.2	57.0	2.8
GOOD-2	77	245.9	−36.9	59.9	1.9	242.5	−56.1	75.3	1.9
BEST	67	245.8	−37.4	61.5	2.2	242.3	−56.7	79.1	2.0

Comments. Name: ALL is for sites based on three samples or more ($n \geqslant 3$).
BAD is for site-means with $\alpha_{95} > 15°$ and/or $n < 4$; GOOD-1 is for site-means with $\alpha_{95} < 15°$ & $n \geqslant 4$; GOOD-1&DG is the mean for 18 directional groups and 29 site-means.
GOOD-2 is as GOOD-1 but site-means with $k < 50$ are excluded too.
BEST is for site-means with $\alpha_{95} < 10°$ & $n \geqslant 4$.
N = the number of sites used, D = declination, I = inclination. k = concentration parameter, α_{95} = radius of confidence circle (Fisher, 1953).

Many theoretical studies (e.g., Tauxe and Kent, 2004, and references therein) treat SV as a stochastic process, and hence any sufficiently long part of a SV record provides unbiased estimates of geomagnetic field characteristics (mean direction, concentration parameter, etc.). If true, then any portion of a long SV record must have statistically similar characteristics provided that the record is not too short. In contrast, parts of a short record will most likely give parameter estimates that are different from those of the entire dataset. In the latter case, the partial values of concentration parameter will tend to be larger than the value for the entire dataset.

This analysis was applied to the GOOD-1 dataset with running windows of 15, 21 and 29 unit vectors that were shifted by a half-window at each step (Fig. 7c). For the smallest window ($N = 15$), all window-mean k values are statistically similar to the overall mean k value, except for the first (= lowermost) subset. For the window of $N = 21$, the first k value is marginally significant, while all others are statistically indistinguishable. Finally, all window-mean k values are statistically similar for the widest window of $N = 29$. Thus it looks possible to conclude that the lowermost part (only) of the section of ~15 sites is "over-grouped", although these unit vectors do not constitute a directional group as defined, for instance, by Chenet et al. (2009). All other window-mean k values conform to the null-hypothesis that each window spans a sufficiently long time interval for SV averaging. As each second window-mean only is an independent result, the conservative conclusion is that the studied section is at least three times longer than is required for adequate SV averaging. Note, however, the NRO factor without the lowermost fifteen sites is 99%, and some undetected regularities may still be hidden in the dataset.

6. Analysis of PSVL data

6.1. Basics

The analysis on PSVL is usually conducted using virtual geomagnetic poles (VGPs). We evaluate PSVL in direction space for the following reasons: (1) It is directional data that are measured and VGPs represent a calculation based on the directional data and (2) the 'mapping function' (i.e. conversion of directional data into VGPs) decreases VGP scatter for low-latitude data and increases it for high-latitude datasets (Merrill et al., 1996). A few directions on the margin of directional distribution may greatly and non-linearly affect the parameters of the entire VGP distribution. This effect is particularly important for small and moderate sets of high-latitude data.

Several SV models have been suggested (e.g., see Tauxe et al., 2008 for review), of which the TK03.GAD model by Tauxe and Kent (2004) appears to be most widely used, provides the largest number of testable parameters and can be tested against a single dataset. An important feature of this model is that it produces a rather large number of anomalous VGPs. A VGP cutoff angle of 45° is commonly used in secular variation studies and yields about 3% anomalous directions (e.g., Deenen et al., 2011). Although 3% appears to be rather minimal, Deenen et al. (2011) show that the concentration parameter k and mean angular deviation s are considerably changed by applying this cutoff, while the values of elongation E are much less affected. To be consistent, one must either apply the same cutoff to both predicted and observed data, or disregard it everywhere; the first option appears to be the common choice.

6.2. Data selection

In order to compare our new result with other pre-Late Cenozoic PSVL data with maximal consistency, dataset selection is important. Below, we list the criteria that must be met by each dataset included in our analysis:

(1) All data are from a limited area, within which, to the best of our knowledge, tectonic rotations are unlikely;
(2) All data are from a stratigraphic interval of a few Ma at most;
(3) All sites are on lava flows, with a few tuffaceous units or dikes being permissible; the results on dyke swarms and multiple dykes were not considered here;
(4) The remanence analyzed is demonstrably near-primary;
(5) All samples from all sites are subjected to detailed stepwise cleaning and principal component analysis of demagnetization data;
(6) Each site-mean is based on stable linear vectors or stable vectors combined with remagnetization-circle trajectories from at least four independently oriented samples. Sites solely based on remagnetization circles were excluded from analysis;
(7) The radius of 95% confidence circle (α_{95}) around the site-mean direction is less than 15°;
(8) Data (directions and VGPs) have a unimodal distribution without clearly visible separate clusters;
(9) Evidence is provided that secular variation, SV, of the geomagnetic field is adequately averaged in the dataset;
(10) The number of acceptable unit vectors N is > 25; directional groups were used as recognized in the original papers, by replacing the corresponding site-means.

There are scores of published paleomagnetic data on lavas, but the last criterion is their most "merciless killer" as many of them are originally based on 10–20 flows, and further selection only

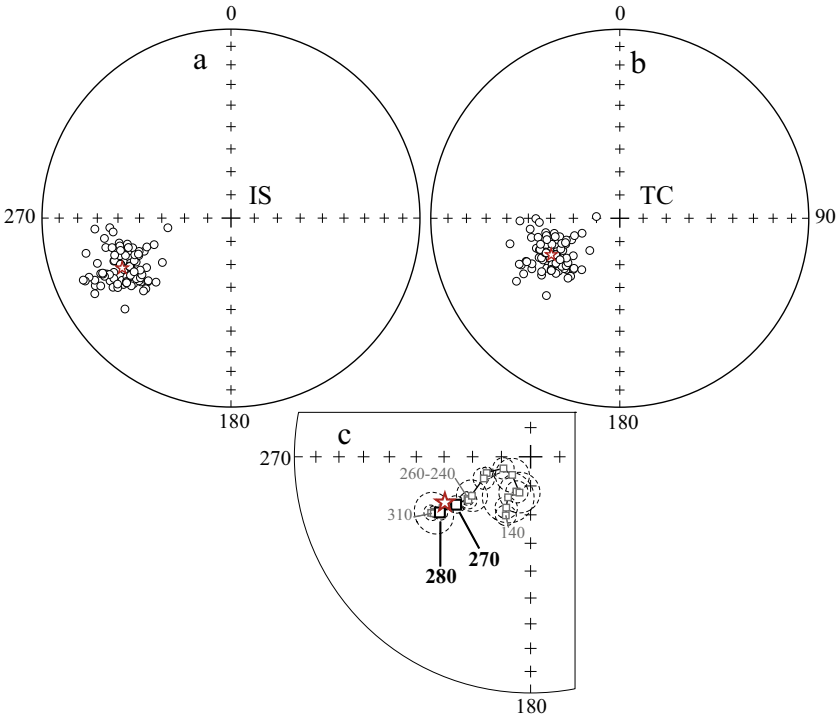

Fig. 6. (a, b) Stereoplots of HTC site-mean directions (circles) in Permian volcanics of the Bakaly Fm. in situ (a) and after tilt correction (b). Confidence circles are omitted for clarity. Only the data classified as BEST (number of samples $n \geqslant 4$, radius of confidence circle $\alpha_{95} < 10°$) are plotted. Red star is the overall mean direction; note that the corresponding confidence circle is less than the symbol. (c) Comparison of the overall mean direction after tilt correction (red star) with the reference directions from Baltica with associated confidence circles (thin dashed lines). These directions are calculated by extrapolation from the apparent polar wander path of Baltica (squares; Torsvik et al., 2012). The directions for 270 Ma and 280 Ma are shown by larger symbols. All symbols and lines are projected onto upper hemisphere. (For interpretation of the references to color in this figure legend, the reader is referred to the web version of this article.)

reduces these modest numbers. Other criteria contribute too. For instance, provision 1 made us discard the studies in tectonically active areas because of local rotations, the numerous data on the Emeishan traps in South China being an example (Zheng et al., 2010). Also "deadly" proved to be provision 8, which made us reject the Tertiary data from West Greenland (Riisager et al., 2003), which form two widely separated tight clusters, thus rendering further analysis worthless. The data on Triassic–Jurassic volcanic piles from Morocco (Knight et al., 2004) fall into a number of tight clusters, and both site- and cluster-means form a long banana-like swath on the stereonet, which is very unlikely to have resulted solely from secular variation. Still other example is the data on the lower and upper parts of the Late Devonian lava pile from Kyrgyzstan that yield two k values that differ about fourfold (Bazhenov et al., 2013).

Using the above criteria, we found twenty-one datasets on thick lava piles of pre-Cenozoic age (Table 3). The original full data sets are given in the Supplement (PSVL-data.xls). Note also that no correction for the within-site scatter is introduced into the k and s values as the required information is not always presented in original publications. These corrections, however, are usually less than 10% for k values and <2° for s, and their omission does not affect the general patterns below.

6.3. Dispersion characteristics: predicted and observed

Dispersion of paleomagnetic directions (or VGPs), which is evaluated either with the concentration parameter k (Fisher, 1953) or mean angular deviation s ($s^2 = 6561/k$), is the most important and "accessible" characteristic. Note that the k parameter has well studied properties for Fisher-distributed data (Mardia, 1972) and can readily be used for statistical tests using tabulated F-distributions. In contrast, differences in the s parameter are more difficult to evaluate and compare in a statistical manner. Since the Fisher distribution is analogous to the normal distribution for 1D statistics, Fisher estimates remain valid in spite of any slight deviations within the analyzed data. Most comparisons of the mean angular deviation (s) are conducted via bootstrapping methods that can give biased estimates (see Tauxe et al., 1991 for discussion).

The most noticeable features on the plot of k versus paleolatitude are the large scatter and scarcity of data from both low (<20°) and high (>65°) latitudes (Fig. 8a). With the sole exception (#5), the observed k values are higher than those predicted by TK03.GAD model without cutoff (thick dashed line in Fig. 8a), the differences being statistically significant in most cases. Bazhenov et al. (2014) compared the observed k values with TK03.GAD predictions and noted poor agreement. Note, however, that the reference data in Bazhenov et al. (2014) r were NOT treated with a cutoff, while a 45° cutoff was applied to the other studies used in that comparison. Hence the conclusion that there is NO match between the observed and predicted values made by Bazhenov et al. (2014) is invalid. In contrast, the model curve after a 45° cutoff (thick red line) fit the data much better, and about 50% of results fall into, or close to, its confidence limits (yellow shading) that are computed for $N = 50$, using the F-distribution.

Quite predictably, the data points become less diffuse when concentration parameter k is replaced by standard angular deviation s (Fig. 8b). The price for this, however, is high: the total variances of predicted k and s values between the equator and pole are >250% and ~60%, respectively. Thus the k-to-s transition suppresses the noise and, at the same time, greatly reduces the real differences. As is the case for the concentration parameter, no correlation can be established between s values and other parameters

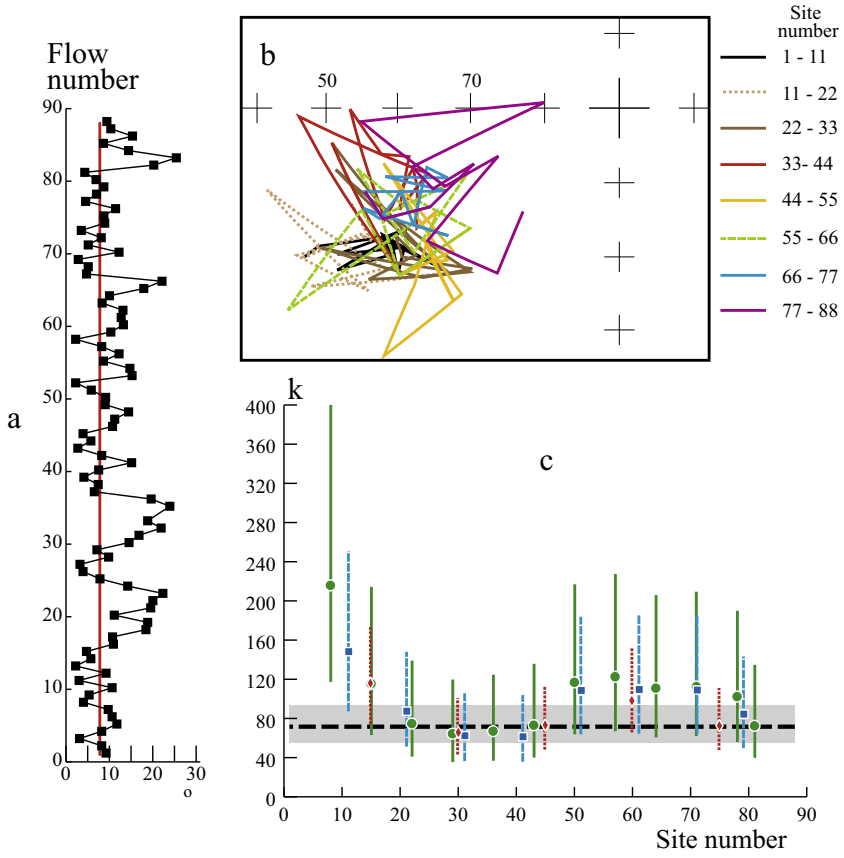

Fig. 7. (a) Plots of angular difference Δ° between adjacent site-mean directions for 88 stratigraphically (top above) ordered site-means. (b) Part of a stereoplot with the trajectory of the site-mean directions for 88 stratigraphically ordered site-means. For better visibility, the site-means themselves are not plotted, but the entire trajectory is divided into eight differently colored segments. (c) Concentration parameter k values for sliding windows of 15 (circles), 21 (squares) and 29 (diamonds) unit vectors. 95% confidence limits for window-mean k values are denoted by vertical bars. Thick dashed line represents the overall mean k value with its 95% confidence limits (shaded). (For interpretation of the references to color in this figure legend, the reader is referred to the web version of this article.)

such as the reversal rate. Any attempts to describe the overall variation of s with paleolatitude (Fig.8b) are hindered by the scarcity of both low- and high-latitude data.

6.4. Form parameters: predicted and observed

The elongation E of directional distributions is an innate property of the mapping function that transforms a circular cloud of poles into an elongated distribution of directions. If the poles have infinitely small dispersion, the elongation will range from 4.0 at the equator to 1.0 at the pole. The larger is the scatter of poles, the less is the E value at the equator (Tauxe et al., 2008). Thus the values predicted by the TK03 model, from ~2.9 at the equator to 1.0 at the pole (Fig. 9a), are fully determined by the prescribed VGP scatter, and the removal of anomalous data with a cutoff only slightly affects the above numbers (Deenen et al., 2011).

The general distribution of E is unknown, and the confidence limits for this parameter have to be determined with bootstrapping, despite a bias that may be present for such estimates; this problem, however, was not thoroughly studied. The variability of E estimates for different sample size was studied with numerical simulations and was found to cover most of, if not the entire, permissible interval (i.e., from 2.9 to 1.0) for this parameter even for sample sizes as large as 200 (Fig. 4 in Tauxe et al., 2008). Still, it was suggested that $N > 100$ data points are necessary for robust estimates (Tauxe, 2005; Tauxe et al., 2008). In spite of the fact that statistical arguments require N values of >100, the need for practicality results in the use of smaller datasets. Even for the largest collections studied the confidence intervals are still very wide (e.g., Fig. 11 in Haldan et al., 2014).

The above study of the variability of E estimates (Tauxe et al., 2008) was carried out without a cutoff. Although Deenen et al. (2011) showed that application of a cutoff slightly affects the average E values, we decided to evaluate the variability E values with and without a 45° cutoff. So data sets of $N = 100$ points each were derived from the TK03.GAD model at latitudes from 0 to 50°. This N value agrees with what was recommended by Tauxe (2005) and is close to the upper limit on the collection size that is attainable in practice (Table 3). Five percent of the largest and lowest E values were discarded for each latitude, and the remaining 90% variability ranges are shown as thick vertical bars both for data without a cutoff and with a cutoff (Fig. 9a). For comparison, variability ranges for collection of $N = 400$ are also shown.

Irrespective of whether or not a cutoff was used, the variability of elongation is similar (red and green bars, respectively, Fig. 9a) and very large, in accord with the earlier findings of Tauxe et al. (2008). Naturally, the variability quickly increases for smaller datasets (Fig. 4 in Tauxe et al., 2008). Only for $N = 400$ does the variability of elongation become reasonably small and allowing for a comparison between the observed data and model predictions.

Given the limitations in available sample sizes, we lowered the threshold to $N \geqslant 50$ for comparison with the observed data. In spite of large dispersion, the data are broadly compatible with the TK03.GAD model or, more accurately, do not contradict it. It should also be noted that these results are also compatible with other SV models (Constable and Parker, 1988; Quidelleur and Courtillot, 1996; Constable and Johnson, 1999).

Table 3
Paleomagnetic data on thick lava series with the ages of >5 Ma.

#	Object	Age	$\varphi°$	$\lambda°$	N	$I°$	$\alpha_{95}°$	Plat°	k	$s°$	E_d	E_p	$D_c°$	$I_c°$	NRO%	A	P	Ref
1	Columbia R. Basalts	16	46	243	**86**	60.7	3.2	41.7	24.4	16.4	2.02	1.12	82.4	−4.4	~99	7	M	[1]
2	Steens Mountain	17	43	242	**50**	59.2	4.2	40.0	24.0	16.7	1.48	1.73	39.5	−24.5	–	0	M	[2]
3	Kerguelen	27	−49	69	**91**	68.4	2.3	51.6	42.5	12.5	1.36	1.21	102.0	−4.7	–	5	M	[3]
4	Yemeni traps	30	16	44	45	1.3	5.9	0.7	14.0	21.9	–	–	–	–	–	2	M	[4]
5	Ethiopia traps	30	13	40	**57**	0.7	6.0	0.4	10.8	25.0	3.78	1.65	89.9	8.3	–	2	M	[5]
6	Faroe Islands	58	62	353	42	60.4	4.6	41.4	25.8	16.1	–	–	–	–	–	1	M	[6]
7	Deccan traps	68	19	73	**73**	46.4	3.7	27.6	20.8	17.9	2.51	1.45	97.7	−7.4	17	16	M	[7]
8	Arctic Canada	95	79	267	33	79.6	3.9	69.8	41.5	12.6	-	-	-	-	-	0	N	[8]
9	Mongolia	120	44	102	**128**	65.9	1.9	48.2	44.9	12.1	1.44	1.12	81.9	−5.6	>99	1	M	[9]
10	Lhasa	126	32	83	**51**	34.5	2.3	19.0	74.3	9.4	2.06	2.5	74.0	−21.8	–	1	N	[10]
11	North Argentina traps	130	−32	296	47	49.5	3.1	30.3	46.2	12.0	–	–	–	–	91	1	M	[11]
12	Parana traps	130	−26	307	35	42.4	2.5	24.5	97.0	8.2	–	–	–	–	86	0	N	[12]
13	Etendeka traps	135	−20	14	**64**	42.2	3.8	24.4	22.6	17.0	1.16	2.35	69.9	29.1	94	0	M	[13]
14	Lesotho traps 1	180	−30	29	47	53.7	3.2	34.2	42.0	12.5	–	–	–	–	>99	0	M	[14]
15	Lesotho traps 2	180	−31	28	20	53.8	4.5	34.3	53.4	11.1	–	–	–	–	>99	0	M	[15]
16	Siberian traps, Norilsk	250	70	90	42	75.4	3.6	62.5	39.0	13.0	–	–	–	–	–	0	M	[16, 17]
17	Siberian traps, Kotuy	250	71	101	26	76.2	3.8	63.8	56.5	10.8	–	–	–	–	96	3	M	[17]
18	Sierra Chica, Argentina	260	−38	295	29	60.9	2.8	41.9	91.5	8.5	–	–	–	–	–	0	M	[18]
19	NE Kazakhstan	280	49	81	**88**	56.2	1.8	36.8	71.5	9.6	1.38	1.28	93.9	−0.5	>99	0	R	[19]
20	Oslo graben	290	60	10	**102**	38.0	2.0	21.3	59.0	10.6	1.22	2.98	58.0	−34.1	–	0	R	[20]
21	Lake Superior	1100	47	269	77	43.8	2.8	25.6	34.3	13.8	2.00	1.07	87.5	2.7	>99	0	M	[21]

is the number of a result as used in the text and figures. Approximate age is in Ma. φ and λ are geographical latitude (negative for the southern hemisphere) and longitude of the object. N is the number of sites and directional groups (bold if >50). Plat is paleolatitude calculated with the dipole formula. s is standard angular deviation; no correction for the within-site scatter was introduced into the k and s values as the required information is not always available. E_d (E_p) is elongation of the unit vector (VGP) distribution. D_c (I_c) is the declination (inclination) of the normal to the great circle that is fitted to the distribution of unit vectors after subtracting the mean declination of the collection. Parameters E_d, E_p, D_c, and I_c are presented for larger collections ($N \geqslant 50$) only. NRO is NRO factor (Biggin et al., 2008a). A is the number of anomalous directions rejected with 45° cut-off applied to VGPs. P is polarity: N, normal; R, reverse; M, mixed. Ref are references: [1], Dominguez and Van der Voo, 2014; [2], Jarboe et al., 2008; [3], Plenier et al., 2002; [4], Riisager et al., 2005; [5], Rochette et al., 1998; [6], Riisager et al., 2002; [7], Chenet et al., 2009; [8], Tarduno et al., 2002; [9], van Hinsbergen et al., 2008; [10], Ma et al., 2014; [11], Geuna and Vizan, 1998; [12], Alva-Valdivia et al., 2003; [13], Dodd et al., 2015; [14], Kosterov and Perrin, 1996; [15], Moulin et al., 2012; [16], Heunemann et al., 2004; [17], Pavlov et al., 2015; [18], Domeier et al., 2011; [19], This study; [20], Haldan et al., 2014; [21] Tauxe and Kodama, 2009. Other notation as in Table 2.

In stereonet space, the elongation will have a meridional orientation for all SV models. Given this geometry, the normal to the great circle passing through the distribution of unit directions must lie on the stereonet equator 90° away from the mean declination (Bazhenov et al., 2014). If the observed normal deviates considerably from the predicted direction, the observed elongation, irrespective of its value, is unlikely to be fully related to secular variation. In order to compare different datasets, the predicted declinations D_c must be standardized with a simple formula: $D_c = D_{gc} - D_{dir}$, where D_{gc} is the observed declination of the normal to the fitting great circle, and D_{dir} is the mean declination for paleomagnetic directions.

We tested this prediction with the same multiple samples of $N = 100$ randomly drawn from the TK03.GAD model. The preferred orientation appears to be tightly followed at latitudes of $\leqslant 22°$ (Fig. 9b), but becomes erratic at latitudes of $\geqslant 30°$ (Fig. 9c). As large datasets ($N = 100$) are very rare in practice, one may expect that this parameter will retain its regularity at latitudes of 30° or less for smaller datasets.

The observed data conform well to the above prediction. Seven out of eleven normals fall into the predicted cluster near the equator. Out of four deviating normals, those for the #2 and #10 datasets are based on marginally acceptable collections ($N = 50$ and 51), and the deviations may be attributed to statistical fluctuations. It is not so with the other two cases (## 13 and 20), with rather low latitudes of ~20° and $N \sim 100$. The somewhat anomalous parameters of the data from the Oslo graben (# 20) have been noted by their authors (Haldan et al., 2014) and accounted for by ca. 7° relative rotations, but this explanation looks less likely for the platformal Etendeka traps (# 13).

Finally, we would like to address the haunting question of geomagnetism: what has a more circular distribution, paleomagnetic directions or VGPs? The prevailing opinion is that the VGP distribution should be perfectly circular (albeit not necessarily Fisherian; Tauxe et al., 2008). This conclusion, however, is based on visual comparison of limited datasets (Creer, 1962; Cox, 1970). Beck (1999) analyzed this problem quantitatively by comparing the elongations for several datasets from cratonic areas and came to conclusion that "VGPs are usually more circular than the corresponding set of directions", but the pattern he observed (Fig. 9 in the cited paper) does not seem either unequivocal or very convincing. It is worth stressing that, out of 13 datasets he used, just one is based on a large collection ($N = 70$), which includes lava, dykes and sediments, and another one is of a smaller size ($N = 31$), while N ranges from 10 to 20 unit vectors for other datasets.

We used Beck's approach for the compiled data with $N \geqslant 50$ (Fig. 9e and Table 3). We found no clear pattern and believe it reflects another manifestation of the innate variability in elongation. We argue that the issue of 'most circular' has no solid observational grounds, and it is possible that neither directions nor poles are perfectly circular (e.g., Linder and Gilder, 2012).

6.5. Distribution of paleomagnetic anomalies

As noted above, the TK03.GAD model predicts that about 3% of the VGPs should be regarded as anomalous if the 45° cutoff is used; sometimes, such an anomalous VGP may be as far from the mean pole as 180°. As all unit vectors in model-produced datasets are independent, the probability that two sequential VGPs will be anomalous is ~0.1% and becomes negligible for three or more VGPs in a row. Note also that there are other sources of paleomagnetic anomalies, like transitional zones and excursions, land-slides, mis-corrected tilts, etc, and the number of anomalous data cannot be less than predicted by the model. So, if several consecutive anomalies are observed in a time series, they likely correspond to a single event. Below, two or more adjacent anomalous data are treated as a single anomaly, irrespective of its origin. Note also that the number of anomalies produced by the TK03.GAD model may vary considerably from sample to sample; for instance, this number varied from 0 to 10 in our simulated samples with $N = 100$.

The number of anomalies for the Cenozoic data (## 1–6) is close to the expected level, i.e. the anomaly ratio is ~4.5%

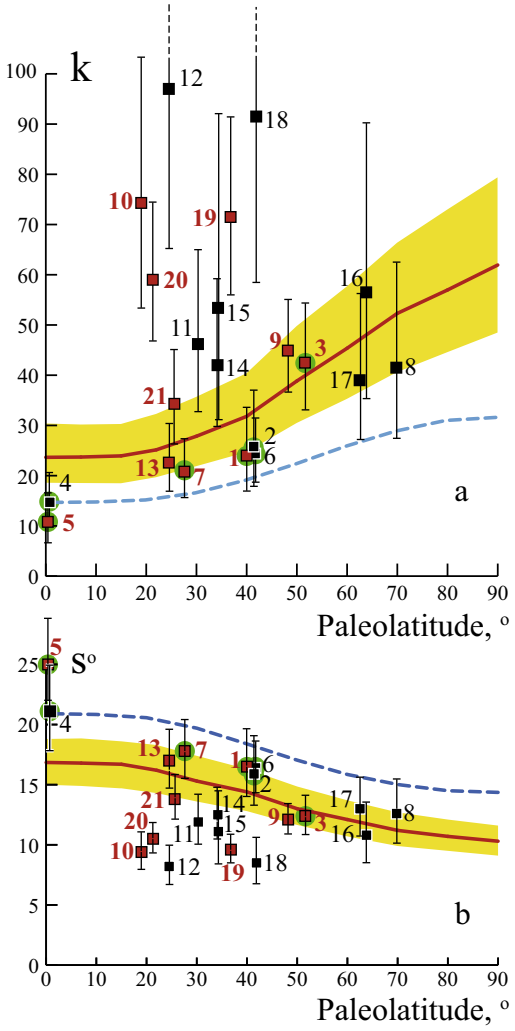

Fig. 8. Plots of (a) concentration parameter k and (b) standard angular deviation, versus paleolatitude. The results are keyed as in Table 3. Red (black) symbols denote the results based on >50 (<50) unit vectors; green circles highlight the data from the Late Cretaceous – Cenozoic interval of high reversal rate. Thin vertical lines denote 95% confidence intervals. Thick dashed blue (solid red) line denotes the prediction of TK03 model from (Tauxe and Kent, 2004) without a cutoff (with a 45° cutoff). Yellow area denotes the 95% confidence interval for the red curve computed for a collection of fifty unit vectors. (For interpretation of the references to color in this figure legend, the reader is referred to the web version of this article.)

(15 anomalies and 314 steady-field entries), and thus is compatible with the TK03.GAD model. This parameter is unusually high for the Deccan dataset (#7), despite the rather narrow stratigraphic interval studied (Chenet et al., 2009). As this interval includes a thick transitional zone, its multiple sampling may account for the larger than average number of anomalous VGPs.

Three datasets (## 8–10) are from the Long Normal Cretaceous Superchron (LNCS). No anomalies were found in Arctic Canada (#8), whereas two sequential anomalous sites in the Lhasa collection (#10) are considered as one anomaly. Biggin et al. (2008a) and van Hinsbergen et al. (2008) reported anomalous directions in the Mongolian collection (#9) and attributed the anomalies to lightning strikes. Our inspection of these data showed that the anomalous directions from two different sections are not random and, moreover, outline rather similar patterns. Given those observations, we treat them as a single anomaly. Thus the anomaly ratio is ~1% during the LNCS (2 anomalies and 212 steady-field entries), which is compatible, albeit barely so, with the TK03. GAD model.

If transitional intervals based on several sequential sites are excluded (e.g., Moulin et al., 2012), there is a single anomaly in one dataset (# 11) and three anomalous data in # 17. In the latter case, the anomalies are likely due to high latitude of the study area: originally, the site- and group-means are rather well clustered ($k = 32$), but three non-adjacent VGPs slightly fall outside of the 45° circle and, formally, are discarded as anomalies. If this contentious dataset is excluded, there is just one anomaly out of >550 data points in eleven pre- LNCS datasets, whereas there should be about fifteen such directions according to the TK03. GAD model. As the anomalies are the inherent property of this model, their nearly total absence may indicate a large change, but of what kind? May it be that the instantaneously acquired thermoremanent magnetization becomes progressively replaced with slower acquired chemical remanences that smooth out short-lived outbursts of the geomagnetic field? Otherwise, could the field generation be more "regular" in the past and hence require a different theoretical description? We do not know.

7. Discussion

The emerging patterns, the dependence of any parameter upon latitude in particular (Fig. 8 and 9), are disappointingly confusing. The results of numerical simulations show that the size of a typical dataset is simply too small to provide robust estimates of the parameters E and D_c (Fig. 9). Hence it is unlikely that these form parameters can be robustly defined from a paleomagnetic collection even as large as 70+ entries.

The elongation–inclination (E/I) method of correcting for inclination shallowing in paleomagnetic data from sediments (Tauxe and Kent, 2004; Tauxe et al., 2008) is based on the statistical properties of the TK03.GAD model. In practice, the E/I method is applied to small datasets of 10 to 30 sites, rarely more, whereas it was conceived for larger datasets. Sometimes, site-means are replaced by sample directions, and the E/I method is used on the sample level to increase the statistics (e.g., Kirscher et al., 2014). This, however, is not correct as the sample directions are not distributed according to the TK03.GAD model. Furthermore, only those elongation parameter values that are less than predicted are used for inclination corrections whereas larger than expected E values are disregarded. Note also that individual estimates of E are highly variable (Fig. 9a). Thus, we contend that the results corrected with the E/I method should be regarded with caution except for extraordinarily large sample sizes (see Tauxe, 2014 for review).

In contrast to the form parameters, the variability of dispersion parameters (k and s) is more than can be accounted for by statistical fluctuations (Fig. 8). It is well known that paleomagnetic data may be clustered due to irregular distribution of volcanism through time. Common analysis of large datasets on lava piles includes identification of directional groups of consecutive site-means with statistically similar directions, which were formed during few centuries; these tightly grouped site-means are replaced with a single group-mean (e.g., Chenet et al., 2009). This does not mean, however, that the directional groups are the only regularities in a PSVL dataset. A visual inspection of such datasets shows that statistically different consecutive unit vectors often form clusters that are more dispersed than directional groups but much tighter grouped than the entire set. The extreme examples of Tertiary data from West Greenland (Riisager et al., 2003) or Triassic-Jurassic lavas from Morocco (Knight et al., 2004) have already been mentioned above, but clusters of 10–15 and more unit vectors may be found in other stratigraphically ordered datasets that superficially look perfectly random. The Bakaly data are not an exception, with at least one cluster detected in the lowermost 10–15 flows (Fig. 7). Note also that archaeomagnetic data

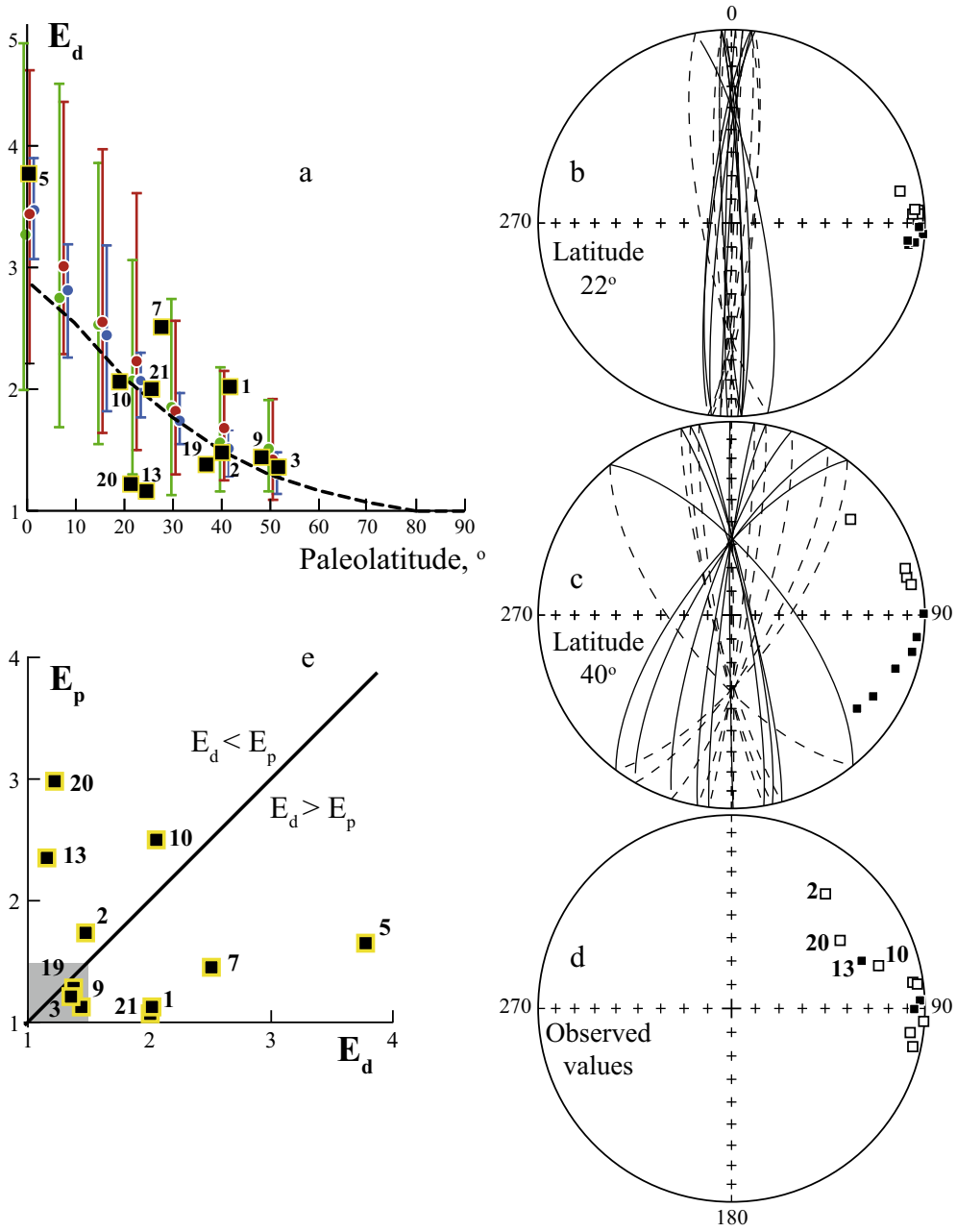

Fig. 9. Analysis of form parameters for simulated and observed data. Black squares are the observed E values (keyed as in Table 3) after a 45° cutoff for the datasets with $N \geqslant 50$. (a) Plot of simulated and observed elongation values E versus paleolatitude. Colored bars and filled circles denote the 90% variability and mean E values, respectively. Green, red and blue symbols denote the original data produced by TK03.GAD for $N = 100$, the same after a 45° cutoff and the results after a 45° cutoff for $N = 400$, respectively. (b–d) Stereoplots of normals (squares) to the great circles fitted to distributions of 100 unit vectors a 45° cutoff for simulated data at the 22° latitude (b), the same at the 40° latitude (c), and the observed datasets (d). For clarity, both great circles and normals to them are shown in (b) and (c); ten randomly chosen entries only are shown. Open (solid) symbols and solid (dashed) lines are projected onto the lower (upper) hemisphere. (e) Plot of elongation E_p of VGP distribution versus elongation of directions E_d. Gray square denotes the area where both parameters are statistically identical to 1 for the datasets of (For interpretation of the references to color in this figure legend, the reader is referred to the web version of this article.).

from many regions for the last two or three millennia (e.g., Gallet et al., 2002; Hagstrum and Blinman, 2010) are systematically tighter grouped than paleomagnetic datasets; in other cases, large loops were identified (Hagstrum and Champion, 1995). Hence such features are likely to occur in sequential paleomagnetic records too.

The assumption that the unit vectors in a dataset are statistically independent can be tested with the NRO factor (Biggin et al., 2008a). To accomplish this analysis, stratigraphically ordered data are needed, either from a single continuous section or several non-overlapping shorter sections. The stratigraphic arrangement of short sections must be definite, as any misalignment causes additional randomness in the data and distorts the NRO results. Of the 21 datasets in Table 3, the NRO could be computed in eleven cases, proved to be significant (>95%) in seven, are close to the critical value for three and is clearly insignificant only once (# 7, Table 3). Thus the basic assumption that the spot-readings of the geomagnetic field are independent and randomly chosen is an oversimplification, as indicated by statistically significant values of the NRO factor for most PSVL data. Unfortunately, this factor tells us that a dataset is not entirely random but does not tell anything about the character of this non-randomness.

The TK03.GAD model was fitted to paleomagnetic data for the last 5 Ma (Tauxe and Kent, 2004), and an important question is if it can be used for older times. There appears to be a tendency for the youngest k values, i.e., those from the Late Cretaceous – Cenozoic interval of frequent reversals (## 1–7, Table 3), either to fit the model or to fall below its predictions (Fig. 8a). The number of the data, however, is limited, and the above tendency may be fortuitous. For older epochs, some data fit the model too, while others do not. No clear regularities are found for the superchron data, and two results (#8–9) from the Cretaceous superchron do not differ from the predictions, whereas the Lhasa datum (#10) is much less dispersed. Two data from the Kiaman superchron (##19–20) are among the least dispersed ones indeed, but are closely matched by the just slightly younger result with the reversals (#18). The larger datasets ($N > 50$) do not show a better consistency, than the smaller ones ($N < 50$; red and black symbols, respectively, in Fig. 8). Even the nearly coeval data from similar paleolatitudes can occasionally disagree with each other as exemplified by the Parana and Etendeka traps (## 11–13).

A basic premise in most analyses of geomagnetic field characteristics is that they do not vary with time, at least not for several million years, as has been assumed by Johnson et al. (2008) in their global compilation of PSVL data for the last 5 Ma. Moreover, many hypotheses, like the relationship between the reversal rate and SV characteristics (Biggin et al., 2008a) or the geomagnetic field evolution since the Archean (Biggin et al., 2008b), are built on the same base. The overall data scatter (Fig. 8a and b), however, seems to be too high to fit into any constant SV value, even with the "aid" of other sources of dispersion. A hypothesis that the SV magnitude may vary several-fold over time intervals of several hundred thousand to few million years has been proposed (Bazhenov et al., 2013). The scatter of PSVL data (Fig. 8) is compatible with this hypothesis; still, it certainly awaits further testing.

8. Conclusions

We densely sampled a nearly monoclinal series of Permian basalt flows in northeast Kazakhstan in order to uncover geomagnetic field characteristics during the PCRS. Magmatic zircons that have been successfully separated from an acid flow in this predominantly basaltic sequence yielded a mid-Early Permian U/Pb age of 286.3 ± 3.5 Ma for these volcanics. Out of 125 flows (= 125 sampled sites), 88 flow-means of high-temperature components were determined with acceptable quality ($n \geqslant 4$ samples, radius of confidence circle $\alpha_{95} \leqslant 15°$). This component is uniformly reversed and of prefolding and most probably primary origin. Its overall mean ($D = 242.0°$, $I = -56.2°$, $k = 71.5$, $\alpha_{95} = 1.8°$, $N = 88$) agrees well with the Early Permian reference paleopoles for Baltica, in accord with the new radiometric age of the lava pile. When compared with PSVL data of various ages, the new Early Permian result indicates a very low level of secular variation with respect to other epochs. The other results, in contrast, are for intervals with high reversal frequencies and display a very high overall scatter of dispersion magnitudes. A correlation between reversal frequency and SV is hinted at, but the scatter of the previously published PSVL magnitudes obfuscates the pattern. The PSVL for the last 5 Myr, for the Miocene, and for the Jurassic, are high, but not uniformly so and cannot be fitted into any particular model. We assume that the main causes for the observed scatter are both statistical nonhomogeneity of the PSVL datasets aggravated by inadequate statistics at each and large variation in SV magnitude on various time scales.

Is it possible to reach a less confusing pattern? In part, yes. In particular, new more elaborate methods of analysis of PSVL datasets are needed. New large PSVL datasets from different paleolatitudes are badly needed for crucial time intervals, for instance, superchrons and the epochs of the highest reversal rate. Unfortunately, there are natural obstacles as well. The continents cover just ~35% of the globe, and their spatial distribution has never been uniform. Even less uniform is the distribution of geological objects through time. For instance, most late Paleozoic large volcanic areas were situated at moderate to high latitudes at that time (Central Asia, east Australia, Argentina), while volcanics are rarer in peri-equatorial regions. Biggin et al. (2008a) noted the scarcity of low-latitude Jurassic data, and the same is evident for the data compiled here (Fig. 8). Hence it is not very likely that suitable objects for PSVL studies can be identified for some geological periods in their entirety, let alone narrower intervals, and the omnipresent slogan of paleomagnetic papers "more data are needed" may remain unfulfilled simply because of lack of objects. Magmatic rocks may be replaced by sedimentary sequences; some attempts of this type have already been undertaken (Kruiver et al., 2000; Haldan et al., 2009), but special thorough studies on very large collections are needed to understand the validity of paleomagnetic record in such rocks.

Acknowledgements

We thank all people from the Scientific Station, Russian Academy of Sciences, in the Bishkek City (Kyrgyzstan), who helped to carry out the fieldworks. Special thanks are due to Nina Dvorova and Olga Krezhovskikh for demagnetization and measurements of the collection. This paper is a product of coordinated efforts of the Russian scientists from Moscow and American researchers from the University of Michigan in Ann Arbor. This study was funded by grants EAR-0909288 (R. Van der Voo) and EAR11-19038 (J. Meert) from the National Science Foundation, grants 12-05-00513 and 15-05-01860 (M. Bazhenov) from the Russian Foundation of Basic Research, contract 14.Z50.31.0017 from the Ministry of Science and Education of the Russian Federation, and by Program # 9, Earth Science Division, Russian Academy of Sciences.

Appendix A. Supplementary data

Supplementary data associated with this article can be found, in the online version, at http://dx.doi.org/10.1016/j.pepi.2016.02.001.

References

Alva-Valdivia, L.M., Goguitchaichvili, A., Urrutia-Fucugauchi, J., Riisager, J., Riisager, P., Lopes, O.F., 2003. Paleomagnetic poles and paleosecular variation of basalts from Paraná Magmatic Province, Brazil: geomagnetic and geodynamic implications. Phys. Earth Planet. Int. 138, 183–196.

Bazhenov, M.L., Grishanov, A.N., Van der Voo, R., Levashova, N.M., 2008. Late Permian palaeomagnetic data east and west of the Urals. Geophys. J. Int. 173, 395–408.

Bazhenov, M.L., Van der Voo, R., Levashova, N.M., Dominguez, A.R., 2013. Late devonian paleomagnetism of the North Tien Shan, Kyrgyzia: Can secular variation vary on a short time scale? Geophys. J. Int. 193, 635–649.

Bazhenov, M.L., Van der Voo, R., Meert, J.G., Levashova, N.M., Ipat'eva, I.S., 2014. Late Paleozoic geomagnetic-field estimates from studies of Permian lavas in northeastern Kazakhstan. Russ. Geol. Geophys. 55, 108–117.

Beck, M.E., 1999. On the shape of paleomagnetic data sets. J. Geophys. Res. 104, 25427–25441.

Biggin, A.J., van Hinsbergen, D.J.J., Langereis, C.G., Straathof, G.B., Deenen, M.H.L., 2008a. Geomagnetic secular variation in the Cretaceous Normal Superchron and in the Jurassic. Phys. Earth Planet. Inter. 169, 3–19.

Biggin, A.J., Strik, G.H.M.A., Langereis, C.G., 2008b. Evidence for a very-long-term trend in geomagnetic secular variation. Nat. Geosci. 1, 395–398.

Chenet, A.-L., Courtillot, V., Fluteau, F., Gerard, M., Quidelleur, X., Khadri, S.F.R., Subbarao, K.V., Thordarson, T., 2009. Determination of rapid Deccan eruptions across the Cretaceous-Tertiary boundary using paleomagnetic secular variation: 2. Constraints from analysis of eight new sections and synthesis for a 3500-m-thick composite section. J. Geophys. Res. 114 (B6), B06103. http://dx.doi.org/10.1029/2008JB005644.

Constable, C.G., Parker, R.L., 1988. Statistics of the geomagnetic secular variation for the past 5 m.y. J. Geophys. Res. 93, 11569–11581.

Constable, C.G., Johnson, C.L., 1999. Anisotropic paleosecular variation models: implications for geomagnetic observables. Phys. Earth Planet. Inter. 115, 35–51.

Cox, A., 1970. Latitude dependence of the angular dispersion of the geomagnetic field. Geophys. J. R. Astron. Soc. 20, 253–269.

Cogné, J.P., 2003. PaleoMac: a Macintosh application for treating paleomagnetic data and making plate reconstructions. Geochem. Geophys. Geosyst. 4 (1), 1007. http://dx.doi.org/10.1029/2001GC000227.

Creer, K.M., 1962. The dispersion of the geomagnetic field due to secular variation and its determination for remote times from paleomagnetic data. J. Geophys. Res. 67, 3461–3476.

Deenen, M.H.L., Langereis, C.G., van Hinsbergen, D.J.J., Biggin, A.J., 2011. Geomagnetic secular variation and the statistics of palaeomagnetic directions. Geophys. J. Int. 186, 509–520.

Domeier, M., Van der Voo, R., Tohver, E., Tomezzoli, R.N., Vizan, H., Torsvik, T.H., Kirshner, J., 2011. New Late Permian paleomagnetic data from Argentina: refinement of the apparent polar wander path of Gondwana. Geochem. Geophys. Geosyst. 12, Q07002. http://dx.doi.org/10.1029/2011GC003616.

Dominguez, A.R., Van der Voo, R., 2014. Secular variation of the Middle and Late Miocene geomagnetic field recorded by the Columbia River Basalt Group in Oregon, Idaho, and Washington, USA. Geophys. J. Int. 197, 1299–1320.

Dodd, S.C., Mac Niocaill, C., Muxworthy, A.R., 2015. Long duration (>4 Ma) and steady-state volcanic activity in the early Cretaceous Paraná-Etendeka Large Igneous Province: new palaeomagnetic data from Namibia. Earth Planet. Sci. Lett. 414, 16–29.

Fisher, R.A., 1953. Dispersion on a sphere. Proc. R. Soc. London Ser. A 217, 295–305.

Gallet, Y., Genevey, A., Le Goff, M., 2002. Three millennia of directional variation of the Earth's magnetic field in western Europe as revealed by archeological artifacts. Phys. Earth Planet. Int. 131, 81–89.

Geuna, S.E., Vizan, H., 1998. New Early Cretaceous paleomagnetic pole from Cordoba Province (Argentina): revision of previous studies and implications for the South American database. Geophys. J. Int. 135, 1085–1100.

Hagstrum, J.T., Champion, D.E., 1995. Late Quaternary geomagnetic secular variation from historical and 14C-dated lava flows on Hawaii. J. Geophys. Res. 100, 24393–24403.

Hagstrum, J.T., Blinman, E., 2010. Archeomagnetic dating in western North America: an updated reference curve based on paleomagnetic and archeomagnetic data sets. Geochem. Geophys. Geosyst. 11, Q06009. http://dx.doi.org/10.1029/2009GC002979.

Haldan, M.M., Langereis, C.G., Biggin, A.J., Dekkers, M.J., Evans, M.E., 2009. A comparison of detailed equatorial red bed records of secular variation during the permo-carboniferous reversed superchron. Geophys. J. Int. 177, 834–848.

Haldan, M.M., Meijers, M.J.M., Langereis, C.G., Larsen, B.T., Heyer, H., 2014. New palaeomagnetic results from the Oslo Graben, a Permian Superchron lava province. Geophys. J. Int. 199, 1554–1571.

Heunemann, C., Krasa, D., Soffel, H.C., Gurevitch, E., Bachtadse, V., 2004. Directions and intensities of the Earth's magnetic field during a reversal: results from the Permo-Triassic Siberian trap basalts, Russia, Earth Planet. Sci. Lett. 218, 197–213.

Jarboe, N.A., Coe, R.S., Renne, P.R., Glen, J.M.G., Mankinen, E.A., 2008. Quickly erupted volcanic sections of the Steens Basalt, Columbia River Basalt Group: secular variation, tectonic rotation, and the Steens Mountain reversal. Geochem. Geophys. Geosyst. 9, Q11010. http://dx.doi.org/10.1029/2008GC002067.

Johnson, C.L., Constable, C.G., Tauxe, L., Barendregt, R.W., Brown, L.L., Coe, R.S., Layer, P.W., Mejia, V., Opdyke, N.D., Singer, B.S., Staudigel, H., Stone, D.B., 2008. Recent investigations of the 0- to 5-Ma geomagnetic field recorded by lava flows. Geochem. Geophys. Geosyst. 9, Q04032. http://dx.doi.org/10.1029/2007GC001696.

Khain, V.E., 1977. Regional Geotectonics (Extra-Alpine Europe and Western Asia). Nedra, Moscow, p. 360, (in Russian).

Kirscher, U., Bilardello, D., Mikolaichuk, A., Bachtadse, V., 2014. Correcting for inclination shallowing of early Carboniferous sedimentary rocks from Kyrgyzstan—indication of stable subtropical position of the North Tianshan Zone in the mid-late Palaeozoic. Geophys. J. Int. 198, 1000–1015.

Kirschvink, J.L., 1980. The least-square line and plane and the analysis of palaeomagnetic data. Geophys. J. Roy. Astron. Soc. 62, 699–718.

Knight, K.B., Nomade, S., Renne, P.R., Marzoli, A., Bertrand, H., Youbi, N., 2004. The Central Atlantic Magmatic Province at the Triassic-Jurassic boundary: paleomagnetic and $^{40}Ar/^{39}Ar$ evidence from Morocco for brief, episodic volcanism. Earth Planet. Sci. Lett. 228, 143–160.

Kosterov, A.A., Perrin, M., 1996. Paleomagnetism of the Lesotho basalt, southern Africa. Earth Planet. Sci. Lett. 139, 63–78.

Kruiver, P.P., Dekkers, M.J., Langereis, C.G., 2000. Secular variation in Permian red beds from Dome de Barrot, SE France. Earth Planet. Sci. Lett. 179, 205–217.

LeGoff, M., 1990. Lissage et limites d incertitude des courbes de migration polaire: Ponderation des donnees et extension bivariate de la statistique de Fisher. C. R. Acad. Sci. Paris Ser. II 311, 1191–1198.

Levashova, N.M., Degtyarev, K.E., Bazhenov, M.L., Collins, A.Q., Van der Voo, R., 2003. Permian paleomagnetism of East Kazakhstan and the amalgamation of Eurasia. Geophys. J. Int. 152, 677–687.

Levashova, N.M., Abrajevitch, A.V., Van der Voo, R., Bazhenov, M.L., 2009. Paleomagnetism of mid-Paleozoic subduction-related volcanics from the Chingiz Range in NE Kazakhstan: the evolving paleogeography of an amalgamating Eurasian supercontinent. Geol. Soc. Am. Bull. 121, 555–573.

Levashova, N.M., Bazhenov, M.L., Degtyarev, K.E., 2012. Oroclinal bending of volcanic belts of Kazakhstan: paleomagnetic evidence and geologic consequences. Geotectonics 46 (4), 285–302.

Linder, J., Gilder, S.A., 2012. Latitude dependency of the geomagnetic secular variation S parameter: a mathematical artifact. Geophys. Res. Lett. 39, L02308. http://dx.doi.org/10.1029/2011GL050330.

Ludwig, K.R., 2008. Manual for Isoplot 3.7: Berkeley Geochronology Center. Special Publication No. 4 77.

Lyapichev, G.F., Seitmuratova, E.Yu., Timofeeva, E.I., Goganova, L.A., 1993. Main problems of the stratigraphy of Late Paleozoic continental volcanics in Central Kazakhstan. In: Milanovskii, E.E. (Ed.), Problems of the Geology and Metallogeny of Central Kazakhstan. Nauka, Moscow, pp. 157–169 (in Russian).

Ma, Y., Yang, T., Yang, Z., Zhang, S., Wu, H., Li, H., Li, H., Chen, W., Zhang, J., Ding, J., 2014. Paleomagnetism and U–Pb zircon geochronology of Lower Cretaceous lava flows from the western Lhasa terrane: new constraints on the India-Asia collision process and intracontinental deformation within Asia. J. Geophys. Res. http://dx.doi.org/10.1002/2014JB011362.

Mardia, K.V., 1972. Statistics of Directional Data. Academic Press, London, p. 357.

McFadden, P.L., McElhinny, M.W., 1988. The combined analysis of remagnetization circles and direct observations in palaeomagnetism. Earth Planet. Sci. Lett. 87, 161–172.

Menzo, Z.M., 2013. Permian Secular Variation of the Ayaguz Formation in Kazakhstan Honors thesis. University of Michigan, p. 28, available at <http://hdl.handle.net/2027.42/97753>.

Merrill, R.T., McElhinny, M.W., McFadden, P.L., 1996. The Magnetic Field of the Earth. Acad. Press, San Diego, p. 527.

Moulin, M., Courtillot, V., Fluteau, F., Valet, J.-P., 2012. The "van Zijl" Jurassic geomagnetic reversal revisited. Geochem. Geophys. Geosyst. 13, Q03010. http://dx.doi.org/10.1029/2011GC003910.

Mueller, P.A., Kamenov, G.D., Heatherington, A.L., Richards, J., 2008. Crustal evolution in the southern Appalachian orogen: evidence from Hf isotopes in detrital zircons. J. Geol. 116, 414–422.

Pavlov, V., Fluteau, F., Veselovskiy, R., Fetisova, A., Llatyshev, A., Elkins-Tanton, L., Sobolev, A., Krivolutskaya, N., 2015. Volcanic pulses in the Siberian Traps as inferred from Permo-Triassic geomagnetic secular variations. In: Schmidt, A., Fristad, K.E., Elkins-Tanton, L.T. (Eds.), Volcanism and Global Environmental Change. Cambridge University Press, Cambridge, pp. 63–78.

Peive, A.V., Mossakovskii, A.A. (Eds.), 1982. Tectonics of Kazakhstan (Explanatory Notes to the Tectonic Map of Eastern Kazakhstan, SCALE 1: 2,500,000). Nauka, Moscow, p. 230 (in Russian).

Plenier, G., Camps, P., Henry, B., Nicolaysen, K., 2002. Palaeomagnetic study of Oligocene (24–30 Ma) lava flows from the Kerguelen Archipelago (southern Indian Ocean): directional analysis and magnetostratigraphy. Phys. Earth Planet. Inter. 133, 127–146.

Quidelleur, X., Couortillot, V., 1996. On low-degree spherical harmonic models of paleosecular variation. Phys. Earth Planet. Int. 95, 55–77.

Riisager, P., Riisager, J., Abrahamsen, N., Waagstein, R., 2002. New paleomagnetic pole and magnetostratigraphy of Faroe Islands flood volcanics, North Atlantic igneous province. Earth Planet. Sci. Lett. 201, 261–276.

Riisager, J., Riisager, P., Pedersen, A.K., 2003. Paleomagnetism of large igneous provinces: case-study from West Greenland, North Atlantic igneous province. Earth Planet. Sci. Lett. 214, 409–425.

Riisager, P., Knight, K.B., Baker, J.A., Peate, I.U., Al-Kadasi, M., Al-Subbary, A., Renne, P.R., 2005. Paleomagnetism and $^{40}Ar/^{39}Ar$ geochronology of Yemeni Oligocene volcanics: Implications for timing and duration of Afro-Arabian traps and geometry of the Oligocene paleomagnetic field. Earth Planet. Sci. Lett. 237, 647–672.

Rochette, P., Tamrat, E., Feraud, G., Pik, R., Courtillot, V., Ketefo, E., Coulon, C., Hoffmann, C., Vandamme, D., Yigru, G., 1998. Magnetostratigraphy and timing of the Oligocene Ethiopian traps. Earth Planet. Sci. Lett. 164, 497–510.

Sal'menova, K.Z., Koshkin, V.Y., 1990. Stratigraphy and Flora of the Late Paleozoic in the North Balkhash Area. Nauka, Almaty, p. 160 (in Russian).

Samygin, S.G., 1974. The Chingiz Strike-slip Fault and its Position in the Structure of Central Kazakhstan. Nauka, Moscow, p. 208 (in Russian).

Shcherbakova, V.V., Shcherbakov, V.P., Sycheva, N.K., Vodovozov, V.Y., 2005. Paleointensity at the Permian-Triassic boundary and in the Late Permian, Izvestiya. Phys. Solid Earth 41, 931–944.

Swanson-Hysell, N.L., Maloof, A.C., Weiss, B.P., Evans, D.A.D., 2009. No asymmetry in geomagnetic reversals recorded by 1.1-billion-year-old Keweenawan basalts. Nat. Geosci. 2, 713–717.

Tarduno, J.A., Cottrell, R.D., Smirnov, A.V., 2002. The Cretaceous superchron geodynamo: observations near the tangent cylinder. PNAS 99, 14020–14025.

Tauxe, L., Kylstra, N., Constable, C., 1991. Bootstrap statistics for paleomagnetic data. J. Geophys. Res. 96, 11723–11740.

Tauxe, L., Kent, D.V., 2004. A simplified statistical model for the geomagnetic field and the detection of shallow bias in paleomagnetic inclinations: Was the ancient magnetic field dipolar? In: Channell, J.E.T., Kent, D.V., Lowrie, W., Meert, J.G. (Eds.), Timescales of the Paleomagnetic Field, AGU Geophys. Monogr., vol. 135, pp. 101–116.

Tauxe, L., 2005. Inclination flattening and the geocentric axial dipole hypothesis. Earth Planet. Sci. Lett. 233, 247–261.

Tauxe, L., Kodama, K.P., Kent, D.V., 2008. Testing corrections for paleomagnetic inclination error in sedimentary rocks: a comparative approach. Phys. Earth Planet. Interiors 169, 152–165.

Tauxe, L., Kodama, K.P., 2009. Paleosecular variation models for ancient times: clues from Keweenawan lava flows. Phys. Earth Planet. Inter. 177, 31–45.

Tauxe, L., 2014. Inclination Shallowing in Sediments: Methods to Account for this and What Do We Do With 'uncorrected' Data in our Databases? Nordic Supercontinent Workshop, Haraldvangen, Norway, October 13–19, 2014. p. 17.

Tevelev, A.V., 2003. Middle-Late Paleozoic Development of the Urals-Kazakhstan Fold System Doctor of Science Thesis. Moscow State University, Moscow, p. 50 (in Russian).

Torsvik, T.H., Van der Voo, R., Preeden, U., Mac Niocaill, C., Steinberger, B., Doubrovine, P.V., van Hinsbergen, D.J.J., Domeier, M., Gaina, C., Tohver, E., Meert, J.G., McCausland, P.J.A., Cocks, L.R.M., 2012. Phanerozoic polar wander, palaeogeography and dynamics. Earth Sci. Rev. 114, 325–368.

Van Hinsbergen, D.J.J., Straathof, G.B., Kuiper, K.F., Cunningham, W.D., Wijbrans, J., 2008. No vertical axis rotations during Neogene transpressional orogeny in the NE Gobi Altai: coinciding Mongolian and Eurasian early Cretaceous apparent polar wander paths. Geophys. J. Int. 173, 105–126.

Zheng, L., Yang, Z., Tong, Y., Yuan, W., 2010. Magnetostratigraphic constraints on two-stage eruptions of the Emeishan continental flood basalts. Geochem. Geophys. Geosyst. 11, Q12014, 12010.11029/12010GC003267.

Zijderveld, J.D.A., 1967. AC demagnetization of rocks: analysis of results. In: Collinson, D.W., Creer, K.M. (Eds.), Methods in Paleomagnetism. Elsevier, Amsterdam, pp. 254–286.